The American Journal of Pathology, Vol. 190, No. 12, December 2020

The American Journal of
PATHOLOGY
ajp.amjpathol.org

CARDIOVASCULAR, PULMONARY, AND RENAL PATHOLOGY

Lymphatic Proliferation Ameliorates Pulmonary Fibrosis after Lung Injury

Peter Baluk,*†‡ Ram P. Naikawadi,§ Shineui Kim,* Felipe Rodriguez,* Dongwon Choi,¶ Young-Kwon Hong,¶ Paul J. Wolters,§ and Donald M. McDonald*†‡

From the Department of Anatomy, the Cardiovascular Research Institute,† the UCSF Helen Diller Family Comprehensive Cancer Center,‡ and the Division of Pulmonary, Critical Care, Allergy and Sleep Medicine,§ University of California, San Francisco, San Francisco; and the Department of Surgery,¶ University of Southern California, Los Angeles, California*

Accepted for publication August 27, 2020.

Address correspondence to Peter Baluk, Ph.D., or Donald M. McDonald, M.D., Ph.D., Department of Anatomy, University of California, San Francisco, 513 Parnassus Ave., San Francisco, CA 94143-0452. E-mail: peter.baluk@ucsf.edu or donald.mcdonald@ucsf.edu.

Despite many reports about pulmonary blood vessels in lung fibrosis, the contribution of lymphatics to fibrosis is unknown. We examined the mechanism and consequences of lymphatic remodeling in mice with lung fibrosis after bleomycin injury or telomere dysfunction. Widespread lymphangiogenesis was observed after bleomycin treatment and in fibrotic lungs of prospero homeobox 1-enhanced green fluorescent protein (Prox1-EGFP) transgenic mice with telomere dysfunction. In loss-of-function studies, blocking antibodies revealed that lymphangiogenesis 14 days after bleomycin treatment was dependent on vascular endothelial growth factor (Vegf) receptor 3 signaling, but not on Vegf receptor 2. *Vegfc* gene and protein expression increased specifically. Extensive extravasated plasma, platelets, and macrophages at sites of lymphatic growth were potential sources of *Vegfc*. Lymphangiogenesis peaked at 14 to 28 days after bleomycin challenge, was accompanied by doubling of chemokine (C-C motif) ligand 21 in lung lymphatics and tertiary lymphoid organ formation, and then decreased as lung injury resolved by 56 days. In gain-of-function studies, expansion of the lung lymphatic network by transgenic overexpression of Vegfc in club cell secretory protein (CCSP)/VEGF-C mice reduced macrophage accumulation and fibrosis and accelerated recovery after bleomycin treatment. These findings suggest that lymphatics have an overall protective effect in lung injury and fibrosis and fit with a mechanism whereby lung lymphatic network expansion reduces lymph stasis and increases clearance of fluid and cells, including profibrotic macrophages. *(Am J Pathol 2020, 190: 2355–2375; https://doi.org/10.1016/j.ajpath.2020.08.018)*

Development of fibrosis is generally thought to be a consequence of disordered wound healing or incomplete resolution of a prior phase of inflammation. Myeloid cells form multiple populations in inflammation, and certain subsets of macrophages are believed to drive fibrosis in the mouse lung bleomycin model[1–3] by inducing other cells to produce collagen.[4] Lymphatics are required for clearance of fluid, immune cells, and mediators from tissues and transport to lymph nodes and undergo conspicuous changes in inflammation.[5–7] Noting that lymphatic growth and immune cell influx are often intimately spatially and temporally related in other inflammatory situations, it was reasoned that lymphatics were likely to be involved in the development and resolution of the inflammatory and fibrotic changes in mouse lungs. To our knowledge, this topic has not been previously examined systematically in lungs.

The role of lymphatics as active contributors to the control of disease severity is receiving greater attention in inflammatory conditions of the skin,[8–10] intestine,[11] heart,[12,13] and brain.[14] Augmented lymphatic function through vascular endothelial growth factor (Vegf) c–driven lymphangiogenesis has been reported either to reduce or to exaggerate inflammation, depending on the disease model,

Supported by NIH/National Heart, Lung, and Blood Institute grants R01 HL059157, R01 HL143896, and R01 HL127402 (D.M.M.); NIH R01 grants HL139897, HL141857 (Y.K.H.), and R01 DK114645 (Y.K.H.); the Harroun Family Foundation grant (P.J.W.), the University of California San Francisco (UCSF) Nina Ireland Program for Lung Health grant (P.J.W.); and the University of California Leadership Excellence through Advanced DegreeS (UC LEADS) program funds (F.R.).

Disclosures: None declared.

https://doi.org/10.1016/j.ajpath.2020.08.018

target organ, and experimental conditions.[15–17] These contrasting effects point to the need for further studies.

Although the influence of lymphatic function on disease severity is less well studied in inflammatory lung conditions, several reports describe changes in lung lymphatics during the course of pulmonary disease in humans and experimental animals.[18,19] Lymphatics undergo conspicuous changes in idiopathic pulmonary fibrosis and other fibrotic lung diseases.[20–22] Similarly, in some bacterial and viral infections, extensive Vegfc-driven lymphangiogenesis accompanies the formation of bronchus-associated lymphoid tissue,[23,24] but the contribution of lymphatic remodeling to severity of lung inflammation has not been examined.

Lymphatic growth promoted by Vegfc can reduce acute rejection of lung allografts.[15] Therapeutic lymphangiogenesis can also ameliorate organ rejection after lung transplantation, and destruction of lymphatics can exacerbate lung disease.[15,25] Functional lymphatic connections are re-established at around 14 days after mouse lung transplantation.[26] However, Vegfc overexpression is also reported to promote innate immune responses and rejection of tracheal allografts.[17,27] This and other evidence from diverse experimental models indicate that Vegfc/Vegf receptor (Vegfr) 3 signaling can shape inflammatory responses in the lung through effects on both lymphatic vessels and immune cells.[17,27]

To explore the contribution of lymphatic vessel remodeling to lung fibrosis and disease severity, the mechanism and consequences of lymphatic remodeling in two mouse models of lung fibrosis were examined. Bleomycin injury was used as a noninfectious model that has been extensively characterized.[28–31] We took advantage of the fact that inflammation and fibrosis are slowly reversible in mouse lungs[32] to look for lymphatic regression. We hypothesized that bleomycin-induced lung injury promotes recruitment of macrophages that are profibrotic, and that expansion of the lung lymphatic network can decrease fibrosis by reducing macrophage accumulation. Because lung fibrosis after bleomycin does not fully mimic idiopathic pulmonary fibrosis in humans,[33] it was determined whether similar changes in lymphatics also occurred in a transgenic mouse model of lung fibrosis driven by telomere dysfunction that more closely resembles pulmonary fibrosis in humans.[34]

This study had three goals. First, we characterized the changes in lymphatics in lung fibrosis. Second, we determined the contributions of plasma leakage, Vegfc/Vegfr3 signaling, and macrophage recruitment to lymphatic growth. Third, we analyzed whether expansion of the lymphatic network in CCSP/VEGF-C double-transgenic mice with an expanded lung lymphatic network[35,36] can reduce lung macrophage accumulation and fibrosis.

Materials and Methods

Mice

Double-transgenic CCSP-rtTA/tetO-VEGF-C (CCSP/VEGF-C) mice of both sexes in C57BL/6 and FVB/N backgrounds were generated by breeding club cell secretory protein reverse tetracycline transactivator (CCSP-rtTA) driver mice (Jackson Laboratory, Bar Harbor, ME; strain 006222, line 1) with tetracycline operator (tetO)-mVEGF-C responder mice.[36] Doxycycline induces rapid, reversible, and dose-dependent transgenic expression of full-length mouse Vegfc in club cells of the airway epithelium and alveolar type II cells, as described.[35,36] Wild-type or single-transgenic (CCSP-rtTA/- or -/tetO-VEGF-C) mice were used as controls. Some CCSP/VEGF-C mice were crossed with Prox1-EGFP mice (Mutant Mouse Regional Resource Center, Davis, CA; strain 031006-UCD; kindly provided by Choi et al[37]) to generate triple-transgenic mice with green fluorescent lymphatics. Cx3cr1-EGFP reporter mice (The Jackson Laboratory; JAX strain 005582) had green fluorescent monocytes, dendritic cells, and macrophages. CCSP-Cre (JAX strain 016225; alias Scgb1a1-CreER) and SPC-Cre (JAX strain 028054; alias Sftpc-CreER^{T2}) mice were bred with TRF1-floxed mice (JAX strain 012336; alias Terf1$^{tm2.1Tdl}$/J) with telomere dysfunction, as described,[34] and were studied at 11 months of age, at which time mortality was increasing. Mice were genotyped by PCR analysis of genomic tail DNA[34,35] and/or by visual examination of bright Prox1-EGFP fluorescence in the lens of the eye.[37] Mice were housed under pathogen-free barrier conditions with ad libitum food and water. For experiments, mice were anesthetized with ketamine (87 mg/kg; Pfizer, New York, NY) and xylazine (10 mg/kg; Bimeda USA, Oakbrook Terrace, IL). Experimental groups had four or more mice, with approximately equal numbers of males and females, except for body weight and survival experiments, where data were collected separately for males and females. The Institutional Animal Care and Use Committee of the University of California, San Francisco, approved all experimental procedures.

Doxycycline Administration

Doxycycline hyclate (1 mg/mL; Sigma, St. Louis, MO; D9891 in drinking water containing 4% sucrose) was given to CCSP/VEGF-C mice from age postnatal day 28 to postnatal day 35 to induce VEGF-C overexpression and lymphatic growth in the lung.[36]

Bleomycin Administration, Body Weight, and Survival

Bleomycin, 2 U/kg (APP Pharmaceuticals, Schaumburg, IL; National Drug Code 63323-136-10), in 50 μL 0.9% NaCl was instilled into the trachea of anesthetized mice of both sexes at 12 to 14 weeks of age through a PE10 polyethylene catheter. Untreated mice were used as controls. After bleomycin administration, survival was monitored on a daily basis, and body weight was measured on alternate days. Peak loss in body weight occurred at 7 to 14 days. In both strains, exaggerated weight loss was predictive of poor survival. Few male FVB/N mice survived the 2 U/kg dose of bleomycin beyond 28 days. Mice with inadequate

bleomycin administration, identified by <10% body weight loss, were excluded from analysis.

Tamoxifen Administration

Tamoxifen (Toronto Research Chemicals, North York, ON, Canada; T006000, suspended in peanut oil) was injected intraperitoneally at a dose of 250 mg/kg body weight once per week to CCSP-Cre/TRF1-floxed and SPC-Cre TRF1-floxed mice and age-matched TRF1-floxed littermate controls for 3 to 9 months beginning at 10 weeks of age, as described.[34]

Treatment with Function-Blocking Antibodies to Block Lymphatic Growth

Function-blocking rat monoclonal antibodies were used to block VEGFR-3 (clone mF4-31C1) and/or VEGFR-2 (clone DC101) (ImClone Systems/Eli Lilly, New York, NY).[23] Blocking antibodies were injected intraperitoneally at a dose of 0.8 mg per mouse in a volume of 200 μL of 0.9% sterile NaCl solution 1 day before bleomycin administration, then every other day for 14 days. Rat IgG (Jackson ImmunoResearch, West Grove, PA; 012-000-003) was used as a control antibody.

Assay of Leukocytes and Protein in BALF

A total of 1 mL of ice-cold Ca/Mg-free phosphate-buffered saline (PBS) containing 5 mmol/L EDTA was flushed up and down via a 22-gauge plastic catheter inserted through the trachea, and then the procedure was repeated once. Leukocytes in bronchoalveolar lavage fluid (BALF) were counted with an automated veterinary hemocytometer (Genesis; Oxford Science Inc., Oxford, CT). For protein assay, BALF was centrifuged at 200 × *g* for 5 minutes to pellet the cells; protein in the supernatant was measured with a bicinchoninic acid protein kit (Thermo/Pierce, Rockford, IL; 23235), according to the manufacturer's instructions using bovine serum albumin standards and read at 562 nm on a spectrophotometer (Biotek, Winooski, VT).

Perfusion, Dissection, and Tissue Collection

Anesthetized mice were perfused for 2 minutes with fixative (1% paraformaldehyde in PBS, pH 7.4) via a cannula inserted through the left ventricle into the aorta. Lungs were inflated at a pressure of 25 mmHg with fixative via a cannula inserted into the trachea, which was then ligated. Lungs were removed and immersed in fixative for 1 hour at room temperature, washed with PBS, infiltrated with 30% sucrose in PBS overnight, and frozen in OCT compound. Bronchial lymph nodes were removed, blotted dry, and weighed.

Immunohistochemistry

Transverse sections of the left lung at the level of the hilum were cut at a thickness of 200 μm with a cryostat.[38] Sections were washed with PBS and stained immunohistochemically with one or more primary antibodies (Table 1) diluted in PBS containing 0.3% Triton X-100, 0.2% bovine serum albumin, 5% normal donkey or goat serum, and 0.1% sodium azide (ImmunoMix[38]). Secondary antibodies were labeled with Cy3, Alexa488, or Alexa647 fluorophores (Jackson ImmunoResearch). Prox1-EGFP proved to be the best marker for imaging lymphatics by fluorescence and confocal microscopy. Lymphatics were identified by VEGFR-3 immunoreactivity in mice that lacked the Prox1-EGFP allele (CCSP/VEGF-C mice, SPC-Cre/TRF1-floxed mice, and SPC/TRF1-floxed mice). The antibody used to determine the distribution of fibrin also recognizes fibrinogen.

Quantitative RT-PCR

Anesthetized mice were perfused with PBS, and the lungs were removed, weighed, and frozen in Trizol (Thermo Scientific, Rockford, IL; 15596026) before extraction of RNA by following the manufacturer's protocol (Thermo Scientific). RNA quality was assessed by a spectrophotometer (Thermo Scientific NanoDrop ND-1000). Samples of 50 ng of total RNA were analyzed by quantitative RT-PCR using SensiFAST SYBR Hi-ROX One-Step Kit (Bioline, Memphis, TN; BIO-73005) and measured in duplicate with a 7300 real-time PCR system (Applied Biosystems, Foster City, CA) using the following protocol: 45°C for 10 minutes, and then 95°C for 2 minutes, followed by 40 cycles at 95°C for 5 seconds and then at 60°C for 30 seconds. Gene expression values were normalized to the housekeeping gene *Sdha*, which, unlike β-actin or glyceraldehyde-3-phosphate dehydrogenase, changes little after bleomycin administration, despite the large influx of inflammatory cells.[39] Results are presented as fold differences between mice treated with bleomycin and untreated controls. PCR primers (Integrated DNA Technologies, Coralville, IA) are listed in Table 2.

Enzyme-Linked Immunosorbent Assay

VEGF-C concentrations were measured using a mouse VEGF-C ELISA Kit (Cusabio, Wuhan, China; CSB-E07361m) following the manufacturer's protocol.

Microarray Profiling in Telomere Dysfunction Model of Lung Fibrosis

SPCcreERT2/TRF1flox/flox mice and *TRF1flox/flox* littermate controls were treated with tamoxifen beginning at 8 weeks of age, as described.[34] Lungs perfused free of blood were removed at age 3 or 9 months. Total RNA, including small RNAs, was extracted using an miRNeasy Mini Kit (Qiagen, Hilden, Germany). Total RNA was measured using a NanoDrop spectrophotometer. All samples passed the quality control parameters established by Agilent (Santa Clara, CA). Agilent mouse microarrays 8 × 60 K v2 (G4852B) were used. Gene expression profiling was performed by Phalanx

Table 1 Antibodies Used for Immunohistochemical Staining of Mouse Lungs

Cells or molecules	Marker	Host	Manufacturer	Catalog no.	Comments
Lymphatic ECs	EGFP in Prox1-EGFP mice	Chicken	Aves (Davis, CA)	GFP 1020	Overall best marker: stains nucleus and cytoplasm
Lymphatic ECs	Prox1	Rabbit	AngioBio (Del Mar, CA)	11-002P	Stains lymphatic ECs, cardiac myocytes, and neuroendocrine cells
		Goat	R&D Systems (Minneapolis, MN)	AF2727	
Lymphatic ECs	Vegfr3	Goat	R&D Systems	AF743	Weaker signal and worse background than Prox1
Lymphatic ECs	Lyve1	Rabbit	AngioBio	11-034	Good in trachea, not in lungs; strongly expressed by some lung blood vessels
		Rat	R&D Systems	MAB2125	
		Goat	R&D Systems	AF2125	
ECs	Pecam1 (Cd31)	Armenian hamster	Thermo Scientific (Rockford, IL)	MA3105	Weaker expression on lymphatic ECs than on blood vessels
		Rat	BioLegend (San Diego, CA)	102502	
ECs	Vegfr2	Goat	R&D Systems	AF644	Vascular ECs and more weakly on lymphatic ECs
High endothelial venules	MECA-79	Rat (IgM)	BD Bioscience (San Jose, CA)	553863	In bronchoalveolar lymphoid tissue
Smooth muscle cells, myofibroblasts	α-Smooth muscle actin (Acta2)	Mouse	Sigma (St. Louis, MO)	F3777 (FITC)	Marks smooth muscle cells of large airways and blood vessels
			Sigma	C6198 (Cy3)	
Type 1 collagen	Type I collagen (Col1a1)	Rabbit	Millipore (Burlington, MA)	AB765P	Used for most staining
		Goat	Southern Biotech (Birmingham, AL)	1310-01	Colocalized with AB765P
Fibrin	Fibrin(ogen)	Rabbit	Dako (Carpinteria, CA)	A0080	Recognizes both fibrin and fibrinogen
Platelets	Integrin a2b Itga2b, Cd41	Rat	BD BioSciences	553847	Clone MWReg30
Leukocytes	Cd45	Rat	BioLegend	103102	Clone 30-F11
T lymphocytes	Cd3e	Armenian hamster	BioLegend	100302	Clone 145-2C11
B lymphocytes	B220	Rat	BioLegend	103202	Clone RA3-6B2
Neutrophils	S100a8	Goat	R&D Systems	AF3059 ab105472	Also known as MRP8 and MRP14
	A100a9	Rabbit	Abcam (Burlingame, CA)		
Macrophages	Aif1/Iba1	Rabbit	WAKO (Richmond, VA); eBioscience (San Diego, CA)	019-19741	Used for most staining
	Cd11b	Rat		14-0112-82	Clone M1/70
	Cx3cr1-EGFP	Chicken		GFP 1020	Antibody to GFP
	Mrc1/Cd206	Rabbit	Aves Bio-Rad (Hercules, CA)	MCA2235GA	Also stains alveolar macrophages and initial lymphatics
Apoptotic cells	Activated caspase-3	Rabbit	R&D Systems	AF835	
VEGF-C	Vegfc	Goat	Santa Cruz (Dallas, TX)	sc-7132	No longer available

Aif, allograft inflammatory factor; EC, endothelial cell; EGFP, enhanced green fluorescent protein; FITC, fluorescein isothiocyanate; GFP, green fluorescent protein; Iba, ionized calcium binding adapter molecule; Lyve, lymphatic vessel endothelial hyaluronan receptor; Pecam, platelet endothelial cell adhesion molecule; Prox, prospero homeobox; VEGF, vascular endothelial growth factor; Vegfr, VEGF receptor.

Biotech (San Diego, CA) using Cy3-labeled antisense RNA for hybridization. Results are expressed as fold differences from corresponding control mice.

Gene Expression in Published Studies

Changes in selected genes retrieved from open access reports of gene expression in mouse lungs after bleomycin challenge (*https://www.ncbi.nlm.nih.gov/geo*; accession numbers GSE37635[40] and GSE40151[41]) or with telomere dysfunction GSE114005[1] were analyzed with GEO2R. Results are expressed as fold differences from values for control mice.

Microscopy, Image Analysis, and Morphometric Measurements

Fluorescence microscopic images of sections (200 μm thick) of left lungs were made by imaging the red and green channels

Table 2 Primers Used for Quantitative RT-PCR of Gene Expression in Mouse Lungs

Molecule	Forward	Reverse
Vegfa	5′-CATCTTCAAGCCGTCCTGTGT-3′	5′-TCTTTCCGGTGAGAGGTCTG-3′
Vegfc (1)	5′-AGCCAACAGGGAATTTGATG-3′	5′-CACAGCGGCATACTTCTTCA-3′
Vegfc (2)	5′-GAAATGTGCCTGTGAATGTACAG-3′	5′-GACAGTCCTGGATCACAATGC-3′
Vegfc (3)	5′-CGTTCTCTGCCAGCAACATTACCAC-3′	5′-CTTGTTGGGTCCACAGACATCATGG-3′
Vegfd (1)	5′-CTGAACAACAGATCCGAGCA-3′	5′-TGCTGAGCGTGAGTCCATAC-3′
Vegfd (2)	5′-GTCTGTAAAGCACCATGTCCGGGAG-3′	5′-CCACAGGCTGGCTTTCTACTTGCAC-3′
Vegfr3	5′-GCTGTTGGTTGGAGAGAAGC-3′	5′-TGCTGGAGAGTTCTGTGTGG-3′
Prox1	5′-CCAGCTGACGAGCTTTTGA-3′	5′-AAATGCAGATGCTGTCCCTAC-3′
Ccl21a	5′-CAACTTGCGGCTGTCCATCT-3′	5′-TTCCGGGGTGAGAACAGGAT-3′
Ccla21b/c	5′-TCCCGGCAATCCTGTTCTTAC-3′	5′-TGGCCGTGCAGATGTAATGG-3′
Actb	5′-GCTCTTTTCCAGCCTTCCTT-3′	5′-CTTCTGCATCCTGTCAGCAA-3′
Hprt1 (1)	5′-CCCAGCGTCGTGATTAGTGATG-3′	5′-TTCAGTCCTGTCCATAATCAGTC-3′
Hprt (2)	5′-CCTCATGGACTGATTATGGACA-3′	5′-ATGTAATCCAGCAGGTCAGCAA-3′
Shra	5′-CTCTTTTGGACCTTGTCGTCTTT-3′	5′-TCTCCAGCATTTGCCTTAATCGG-3′
Ppia	5′-CCAAACACAAATGGTTCCCAGT-3′	5′-ATTCCTGGACCCAAAACGCT-3′

separately at ×5 with an Olympus (Tokyo, Japan) DX73 camera on a Zeiss Axiophot fluorescence microscope (Oberkochen, Germany). Panoramas of whole lung lobes were constructed with the Photomerge function of Photoshop.[38] As cardiac muscle of pulmonary veins has moderate Prox1-EGFP immunofluorescence, these regions were masked in Photoshop before image analysis. The contrast and brightness of the green channel (lymphatics stained for Prox1-EGFP) was adjusted to maximize the contrast between foreground and background. Panoramas were imported into ImageJ software version 1.53d (NIH, Bethesda, MD; *http://imagej.nih.gov/ij*), and the region of interest was traced freehand to outline the whole lung, hilum, or region of parenchyma with the greatest density of lymphatics. Immunohistochemically stained lymphatics in the region of interest with fluorescence intensities above a threshold of 30 (intensity range, $0 < 255$) were expressed as an area density (above threshold pixels as a percentage of total pixels).

Type I collagen was assessed in panoramas of fluorescent images of immunohistochemically stained lungs imaged at the same magnification (×5), contrast, and brightness. The maximum difference between cumulative frequency curves of fluorescence intensities, calculated as intensity = 30 (range, $0 < 255$), was used as the threshold to distinguish foreground from background. The amount of type I collagen immunoreactivity was expressed as the proportion of pixels above this threshold (area density, %).

Allograft inflammatory factor 1/ionized calcium binding adapter molecule 1–stained macrophages and S100a8-stained neutrophils were quantified by using the counting tool of ImageJ on confocal images (40× Zeiss oil-immersion objective number 440756; z-stack depth of 10 μm) of parenchymal hot spots of inflammation in thick sections of lungs after bleomycin treatment, and their numerical density was expressed as cells per mm^2.

Hydroxyproline Assay

–Lungs were removed and frozen at −20°C. The right lungs were homogenized in 1 mL of water, and aliquots were used to measure hydroxyproline with a Sigma MAK008 assay kit for total lung collagen, according to the manufacturer's instructions. The OD of sample wells in 96-well plates was read at 560 nm on a Biotek spectrophotometer. Results were expressed as micrograms of hydroxyproline per whole right lung.

Statistical Analysis

Data are expressed as means ± SEM. Differences between groups were assessed for statistical significance by analysis of variance followed by the Dunnett multiple-comparison test or by *t*-test using GraphPad Prism 6 software (GraphPad Software, San Diego, CA) with $P < 0.05$. Differences between body weight curves and frequency distributions were assessed using the Kolmogorov-Smirnov test. Kaplan-Meier survival curves were assessed using the Mantel-Cox log-rank test. The number of mice in experimental groups is shown in figure legends.

Results

Changes in Lung Lymphatics in Models of Pulmonary Fibrosis

Remodeling of Lung Lymphatics after Bleomycin-Induced Injury

Consistent with other reports,[18,38] lymphatics in lungs of normal C57BL/6 mice accompanied the airways and large blood vessels (Figure 1A). Few lymphatics identified by Prox1-EGFP immunoreactivity were located in the lung parenchyma or pleura, apart from those near conducting airways and blood vessels. The temporal and spatial effects of bleomycin on the lung lymphatic network were assessed by examining the lungs from 0 to 56 days after injury (Figure 1, B–F). Lung lymphatics appeared normal at 7 days, but they were conspicuously changed at 14 days and enlarged near airways and vessels in the hilum and were also abundant in the lung parenchyma and pleura (Figure 1, B and E). Lymphatic remodeling was patchy in the lung parenchyma (Figure 1B) and coincided with regions of inflammatory cell infiltration

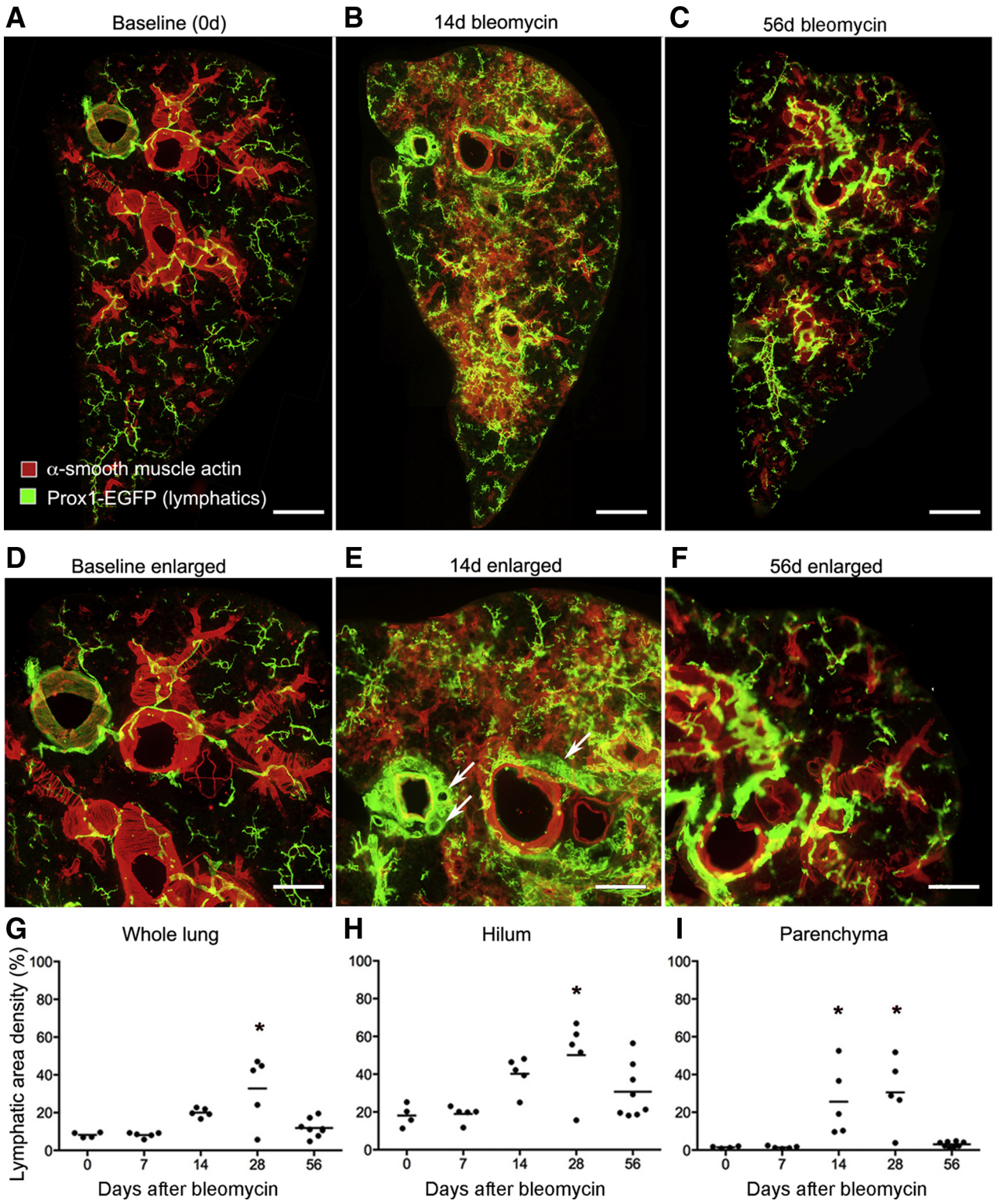

Figure 1 Time course of lymphatic growth in lungs after bleomycin injury. **A**–**C:** Lung panoramas made from tiled low-magnification fluorescence images of sections (200-μm thick) of left lungs of C57BL/6 prospero homeobox 1-enhanced green fluorescent protein (Prox1-EGFP) mice after a single dose of bleomycin. Compared with the control lung (**A**), lymphatics are larger and more numerous around major airways and blood vessels and in the lung parenchyma at 14 days after bleomycin administration (**B**). Lymphatics are less numerous at 56 days (**C**). **D**–**F:** Enlargements of regions in **A**–**C.** Enlargement of collecting lymphatics (**arrows**) around bronchus and pulmonary vein. **G**–**I:** Abundance of lymphatics (area densities) in whole lung, hilum, and parenchyma. Dots represent individual mice. $n = 4$ to 8 mice per group (**G**–**I**). $^*P < 0.05$ versus day 0 (analysis of variance). Scale bars: 1 mm (**A**–**C**); 500 μm (**D**–**F**).

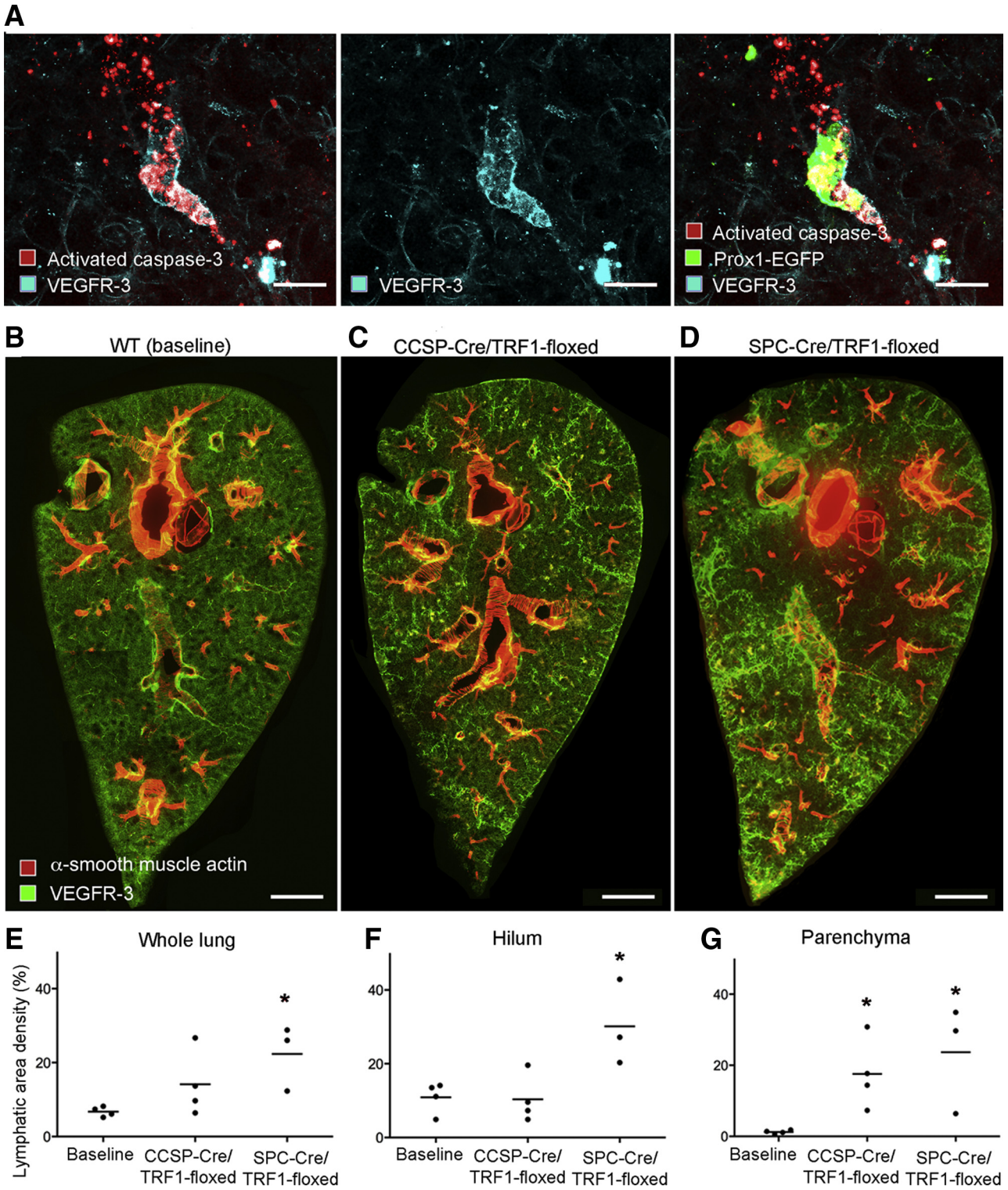

Figure 2 Lung lymphatics: Apoptosis during recovery after bleomycin treatment and network expansion with telomere dysfunction. **A:** Activated caspase-3 staining in and around lung lymphatics stained for prospero homeobox 1-enhanced green fluorescent protein (Prox1-EGFP) and vascular endothelial growth factor receptor (VEGFR)-3 at 56 days after bleomycin administration. **B**—**D:** Low-magnification panoramas of sections (200 μm thick) of left lungs of 9-month—old mice with telomere dysfunction stained for lymphatics (green) and smooth muscle (red). **B:** Baseline [wild-type (WT) littermate]. **C:** CCSP-Cre/TRF1-floxed mouse. **D:** SPC-Cre/TRF1-floxed mouse. **E**—**G:** Abundance of lymphatics (area density) overall and in hilum and parenchyma in baseline mice, CCSP-Cre/TRF1 mice, and SPC-Cre/TRF1 mice. Dots represent individual mice. $n = 3$ to 4 mice per group (**E**—**G**). *$P < 0.05$ versus baseline (analysis of variance). Scale bars: 50 μm (**A**); 1 mm (**B**—**D**).

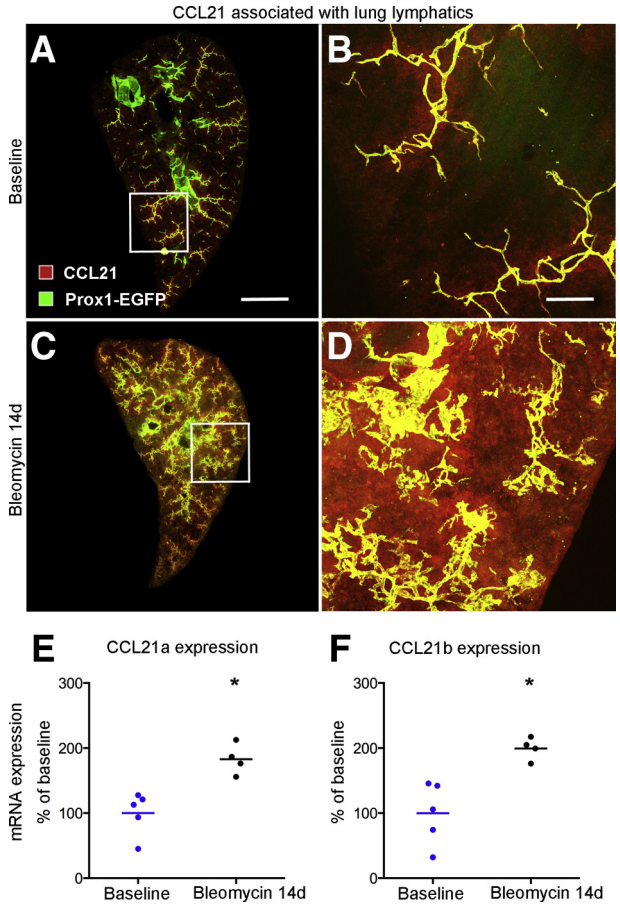

Figure 3 Chemokine (C-C motif) ligand (Ccl) 21 associated with lung lymphatics. **A:** Low magnification of a section (200 μm thick) through left lung at baseline (no bleomycin) stained for Ccl21. **B:** Enlargement of **boxed area** in **A**. **C:** Lung at 14 days after bleomycin challenge, showing Ccl21 immunoreactivity in and diffusely around lymphatics in the lung parenchyma. **D:** Enlargement of **boxed area** in **C**. **E** and **F:** Expression of *Ccl21a* and *Ccl21b* genes, measured by quantitative RT-PCR, in lungs at baseline (blue dots, wild type, day 0) and at 14 days after bleomycin administration (black dots). Dots represent individual mice. $n = 4$ to 5 mice per group (**E** and **F**). $^*P < 0.05$ versus baseline (*t*-test). Scale bars: 1 mm (**A** and **C**); 200 μm (**B** and **D**). Prox1-EGFP, prospero homeobox 1-enhanced green fluorescent protein.

(data not shown). Expansion of the lymphatic network of the lung hilum, parenchyma, and pleura after bleomycin administration was particularly conspicuous in three-dimensional images of optically cleared whole lungs after Prox1-EGFP-immunostaining (Supplemental Figure S1). Similar changes in lung lymphatics were found in FVB/N mice after exposure to bleomycin (Supplemental Figure S2).

In normal mouse lungs, lymphatics were most abundant in the hilum and least numerous in the peripheral lung parenchyma (Figure 1, G–I). Measurements of the density of Prox1-EGFP lung lymphatics at 0, 7, 14, 28, and 56 days after bleomycin treatment revealed a time-dependent increase that varied in different regions of the lung (Figure 1, G–I). Although no change in lymphatic density was detected in the lung hilum or parenchyma at 7 days, the increase in the lung parenchyma was significant at 14 days and was significant in all lung regions at 28 days (Figure 1, G–I). Lymphatics were most abundant in the hilum near large airways and blood vessels at all time points (Figure 1H). However, the proportionate increase was greater in the lung parenchyma (20-fold increase) than in the hilum (threefold increase) (Supplemental Figure S3A), because parenchymal lymphatics were sparse at baseline (area density, approximately 1%).

The question of whether lung lymphatics eventually regressed when the bleomycin injury resolved was addressed by comparing the lymphatic density at the 28-day peak with the value at 56 days. The lymphatic density at 56 days tended to be less in the hilum (Figure 1H) but was significantly less and near baseline in the lung parenchyma (Figure 1I). Although the mechanism of lymphatic regression in the lung parenchyma was not directly assessed, evidence of colocalization of activated caspase-3 and VEGFR-3 immunoreactivity in cell fragments was found in the lung parenchyma at 56 days, consistent with lymphatic endothelial cell apoptosis (Figure 2, A–C).

Remodeling of Lung Lymphatics in Pulmonary Fibrosis due to Telomere Dysfunction

Because the changes after bleomycin injury do not mimic all of the features of human idiopathic pulmonary fibrosis, it was determined whether lymphatic remodeling also occurred in lung fibrosis associated with telomere dysfunction.[34] C57BL/6 mice carrying the CCSP-Cre promoter or SPC-Cre promoter were bred with responder mice carrying the floxed telomere shelterin subunit protein complex (Trf1) gene to produce double-transgenic mice lacking *Trf1*, which develop lung fibrosis over several months.[34] Lungs of both double-transgenic genotypes had greater lymphatic density than age-matched controls (Figure 2, B–D). Lymphatics were more numerous in the lung hilum of SPC-Cre/TRF1 floxed mice and were greatly increased in the lung parenchymal of both types of *Trf1*-deficient mice (Figure 2, E–G). Unlike the effects of bleomycin, *Trf1* deletion had a gradual effect on lung lymphatics, as changes were not evident at 4 months of age but were widespread at 9 months (Figure 2, E–G). Most of the increase in lung lymphatics in CCSP-Cre/TRF1-floxed and SPC-Cre/TRF1-floxed mouse lungs coincided with regions of fibrosis, reflected by aberrant staining for type I collagen and α-smooth muscle actin (Supplemental Figure S3, B–G).

Ccl21 Expression and Immune Cell Influx Accompanying Lymphatic Remodeling

Chemokine (C-C motif) ligand (Ccl) 21, expressed by lymphatic endothelial cells, is a ligand for Ccr7 that promotes entry and trafficking of $Ccr7^+$ dendritic cells to lymph nodes.[42,43] Because of these properties, changes in Ccl21 were assessed as lung lymphatics underwent remodeling after bleomycin challenge. Most Ccl21 immunoreactivity in normal lungs was associated with lymphatics (Figure 3, A and B). At 14 days after bleomycin treatment, when lymphatics were abundant, Ccl21 staining was conspicuously greater, in both lymphatics and surrounding regions of lung (Figure 3, C and D). These changes fit with the finding of greater expression of *Ccl21a* and *Ccl21b* in the lung at

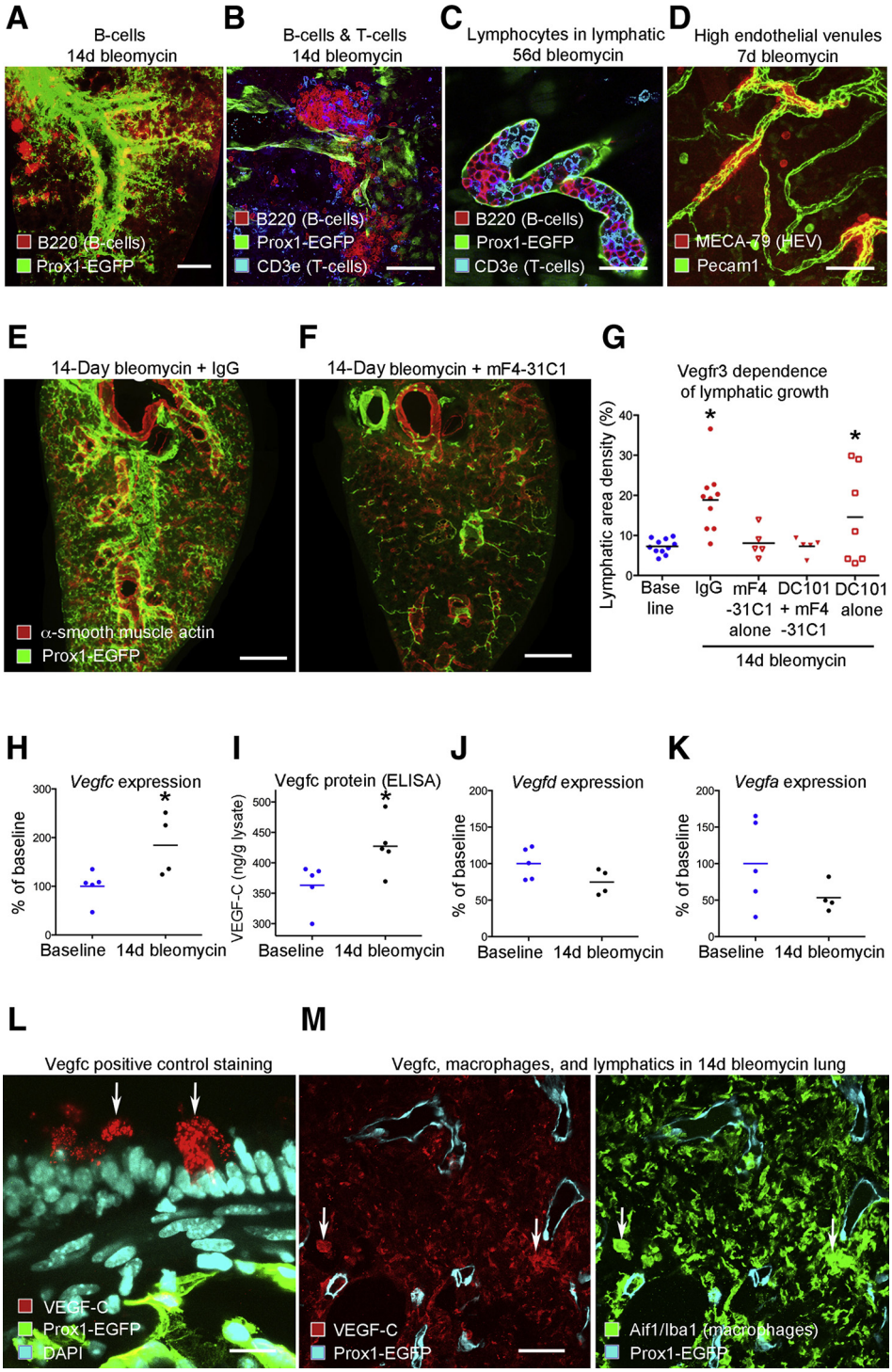

Figure 4 Lung lymphatics associated with lymphocyte influx and dependence on vascular endothelial growth factor receptor (Vegfr) 3 signaling and Vegfc expression. **A:** Lung lymphatics (green) near B-cell follicles (red) in lymphoid tissue near pulmonary vein (bleomycin, 14 days). **B:** Lymphatics near B and T cells in follicles (bleomycin, 14 days). **C:** Lung lymphatic packed with B and T cells (bleomycin, 56 days). **D:** Lymphatics near high endothelial venules (HEVs; MECA-79 staining) in lung hilum (bleomycin, 7 days). **E** and **F:** Low-magnification panoramas of C57BL/6 lung lymphatics 14 days after bleomycin administration without (**E**) or with concurrent Vegfr3 blockade by mF4-31C1 (**F**). **G:** Abundance of lung lymphatics (area density) at baseline (blue dots) or 14 days after bleomycin treatment with concurrent treatment (red symbols) with IgG, mF4-31C1 (anti-Vegfr3), DC101 (anti-Vegfr2), or both antibodies. Symbols or dots represent individual mice. **H**–**K:** Increased expression of *Vegfc* mRNA (quantitative RT-PCR) and protein [enzyme-linked immunosorbent assay (ELISA)] 14 days after bleomycin administration (black dots) without changes in expression of *Vegfd* or *Vegfa* (quantitative RT-PCR) over baseline group (blue dots). **L:** Positive control staining for Vegfc to validate antibody. Triple-transgenic prospero homeobox 1-enhanced green fluorescent protein (Prox1-EGFP)/CCSP/VEGF-C mouse given doxycycline for 7 days to induce Vegfc in epithelial club cells (**arrows**) in bronchus. **M:** Staining for Vegfc, macrophages [allograft inflammatory factor 1/ionized calcium binding adapter molecule 1 (Aif1/Iba1)], and lymphatics in 14-day bleomycin lung. Macrophages (**arrows**) stain for Vegfc. $n = 4$ to 10 mice per group (**G**). $^*P < 0.05$ versus baseline (*t*-test). Scale bars: 1 mm (**A**, **E**, and **F**); 100 μm (**B** and **D**); 50 μm (**C** and **M**); 20 μm (**L**). Pecam1, platelet endothelial cell adhesion molecule.

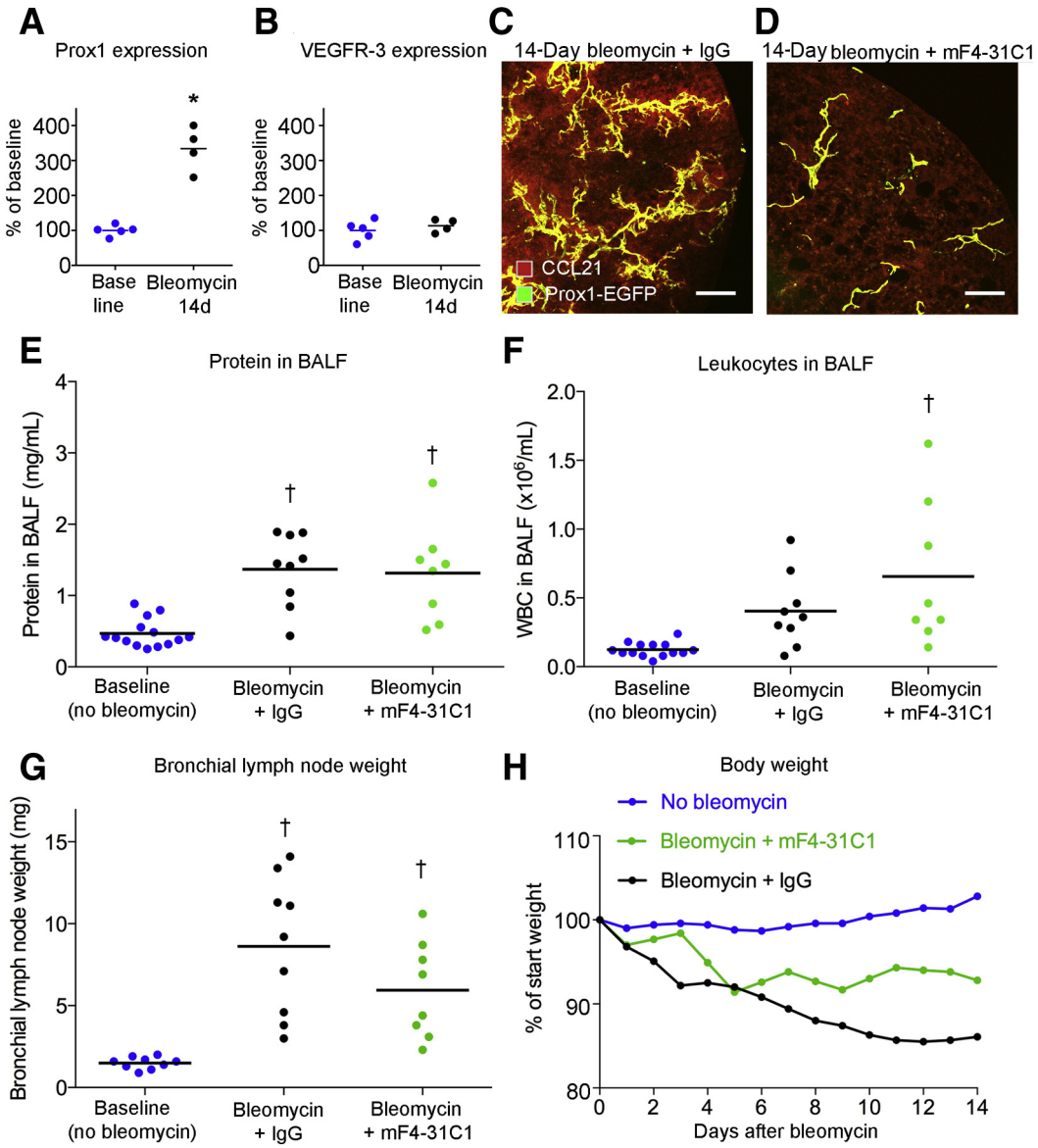

Figure 5 Vascular endothelial growth factor receptor (Vegfr) 3 dependency of lymphatic growth and chemokine (C-C motif) ligand (Ccl) 21 expression but not of bronchoalveolar lavage fluid (BALF) indexes of lung inflammation. **A** and **B:** Expression of *Prox1* and *Vegfr3* (quantitative RT-PCR) in lungs at baseline and 14 days after bleomycin administration. **C** and **D:** CCL21 immunoreactivity in lungs at 14 days after bleomycin challenge, showing large increase in staining when accompanied by control antibody (IgG) but suppression of lymphatic growth and CCL21 staining when accompanied by mF4-31C1 (anti-Vegfr3). **E**–**G:** Lack of difference in BAL protein (**E**), leukocytes (**F**), and bronchial lymph node weight (**G**) of mice given bleomycin with control IgG or mF4-31C1 (anti-Vegfr3). Dots represent individual mice. Blue dots, baseline (no bleomycin); black dots, 14-day bleomycin + IgG; green dots, 14-day bleomycin + mF4-31C1 anti-Vegfr3 antibody. **H:** Body weights of same groups of mice are significantly different from one another ($P < 0.0025$, Kolmogorov-Smirnov test). Dots represent means of groups. $n = 4$ to 20 mice per group (**E**–**G**); $n = 20$ no bleomycin (**H**); $n = 7$ bleomycin + mF4-31C1 (**H**); $n = 9$ bleomycin + IgG (**H**). $^{*}P < 0.05$ versus baseline (*t*-test); $^{\dagger}P < 0.05$ versus baseline (analysis of variance). Scale bars = 200 μm (**C** and **D**). Prox1-EGFP, prospero homeobox 1-enhanced green fluorescent protein; WBC, white blood cell.

14 days (Figure 3, E and F). Similar increases in *Ccl21a* and *Ccl21b* expression are reported in published open-access gene array studies of mouse lungs after bleomycin exposure (*https://www.ncbi.nlm.nih.gov/geo*; accession numbers GSE37635 and GSE40151)[40,41] (Supplemental Figure S4, A and B) and in lung fibrosis accompanying telomere dysfunction (*https://www.ncbi.nlm.nih.gov/geo*; accession number GSE114005)[1] (Supplemental Figure S4C).

To build on the conspicuous association of increased Ccl21 with lung lymphatic remodeling after bleomycin challenge, the relationship of lymphatics to regions of lymphocyte influx was examined. Unlike normal lungs, lymphocytes were abundant in scattered regions of lung after bleomycin challenge, as described in many other reports.[30,31] At 14 days after bleomycin, B-cell follicles, with characteristics of tertiary lymphoid organs,[25] were located near large airways and pulmonary veins (Figure 4, A and B). Lymphatics, some containing lymphocytes (Figure 4C), were particularly numerous around collections of immune cells, which also contained high endothelial venules (Figure 4D).

Mechanism of Lymphatic Growth after Lung Injury

Contribution of Vegfr3 Signaling to Lymphangiogenesis after Bleomycin Challenge

To determine whether lymphatic growth after bleomycin treatment was driven by Vegfr3 signaling, as under many other conditions,[44] lung lymphatics were examined in C57BL/6 mice at 14 days after bleomycin administration, with or without concurrent inhibition of Vegfr3 signaling by function-blocking antibody mF4-31C1. Controls received bleomycin and control antibody (normal rat IgG). Lymphatics in lungs of bleomycin-challenged mice given the Vegfr3 blocking antibody were similar in abundance to those in normal mice, in sharp contrast to the extensive lymphangiogenesis in lungs of controls given bleomycin and control IgG (Figure 4E). In the presence of mF4-31C1, lymphatic growth after bleomycin was suppressed throughout the lung to the baseline level (Figure 4F). Lymphatic growth suppression by mF4-31C1 was not amplified by concurrent inhibition of Vegfr2 by DC101 (Figure 4G). Inhibition of Vegfr2 alone did not suppress the increase in lung lymphatics after bleomycin challenge (Figure 4G).

Increased VEGF-C Expression after Bleomycin Challenge

Vegfc and Vegfd are potent lymphangiogenic growth factors acting via Vegfr3 signaling.[5,45] To determine whether changes in expression of these growth factors coincide with lymphatic proliferation, *Vegfc* and *Vegfd* expression was measured by quantitative RT-PCR at 14 days after bleomycin administration. *Vegfc* expression after bleomycin challenge was twice the control value (Figure 4H). A corresponding increase in Vegfc protein was found by enzyme-linked immunosorbent assay measurements (Figure 4I). Expression of *Vegfd* and *Vegfa* was not increased after bleomycin administration (Figure 4, J and K).

Staining for Vegfc in Macrophages after Bleomycin Challenge

In evidence of the specificity of the Vegfc antibody, as expected, immunohistochemical staining was observed in granules of bronchial epithelial clubs cells of positive-control CCSP/VEGF-C mice treated with doxycycline (Figure 4L). In mice 14 days after bleomycin challenge, moderate staining for Vegfc was found in some interstitial macrophages close to lymphatics (Figure 4M). No staining was found in baseline lungs or in negative-control lungs where the primary anti-Vegfc antibody was omitted (data not shown).

Changes in Other Lymphatic Genes and Conventional Readouts of Lung Inflammation

As a reflection of the increased number of lymphatics, *Prox1* expression was also greater (Figure 5A), but *Vegfr3* expression was not (Figure 5B). To set these data into perspective, these values were compared with changes reported for the time course of gene expression in mouse lungs after bleomycin treatment in published open-access gene array studies (*https://www.ncbi.nlm.nih.gov/geo*; accession numbers GSE37635 and GSE40151[40,41]). After bleomycin challenge, VEGF-C expression was significantly greater in the lung in both data sets (Supplemental Figure S4, A and B). Expression of *Vegfa* and *Vegfr3* was unchanged, and changes in expression of *Vegfd* and *Prox1* were variable, as were the values for housekeeping genes used as a reference (Supplemental Figure S4).

Ccl21 Amplification Blocked by VEGFR-3 Inhibition

VEGFR-3 influences immune cell trafficking by regulating *Ccl21* expression in lymphatic endothelial cells.[43] To expand on the finding of much greater Ccl21 immunoreactivity associated with lung lymphatics after bleomycin challenge (Figure 3, B and D), it was determined whether the increase in Ccl21 was prevented by blocking the proliferation of lung lymphatics after bleomycin treatment. Loss-of-function experiments revealed that lymphatic network expansion and increased Ccl21 staining in and around lung lymphatics did not occur when Vegfr3 was blocked by the mF4-31C1 antibody (Figure 5, C and D).

Influence of VEGF Receptor Signaling on Disease Severity

Multiple indices of disease severity after bleomycin challenge were used to determine the impact of suppression of lymphatic growth. No consistent differences were found in BALF protein at 14 days after bleomycin administration, with or without concurrent inhibition of Vegfr3 signaling by antibody mF4-31C1 (Figure 5E). BALF leukocytes tended to be more numerous, and bronchial lymph node weight tended to be less, but neither difference was significant, as the values had considerable variability (Figure 5, F and G). Bleomycin-challenged mice with Vegfr3 inhibition had less body weight loss after bleomycin than controls treated with IgG (Figure 5H), but overall survival was about the same, regardless of whether the mice received mF4-31C1 or control IgG (Supplemental Figure S5A).

By comparison, inhibition of VEGFR-2 alone was accompanied by more severe disease after bleomycin challenge. C56BL/6 mice that received bleomycin and DC101 to block Vegfr2 had the greatest mortality and highest BALF protein levels and BALF leukocytes at 14 days (Supplemental Figure S5, A–C). With Vegfr2 blockade, α-smooth muscle actin–stained myofibroblasts were twice as extensive in the lung parenchyma after bleomycin challenge (Supplemental Figure S5D). Lung myofibroblasts have been considered as precursors in fibrosis after bleomycin challenge, but are regarded as an imperfect marker of collagen-producing cells.[4,46] Compared with inhibition of VEGFR-2 alone, inhibition of Vegfr2 together with Vegfr3 was accompanied by fewer BALF leukocytes and less mortality after bleomycin administration, indicating that adverse effects of Vegfr2 blockade were reduced by inhibiting Vegfr3 (Supplemental Figure S5, A and C).

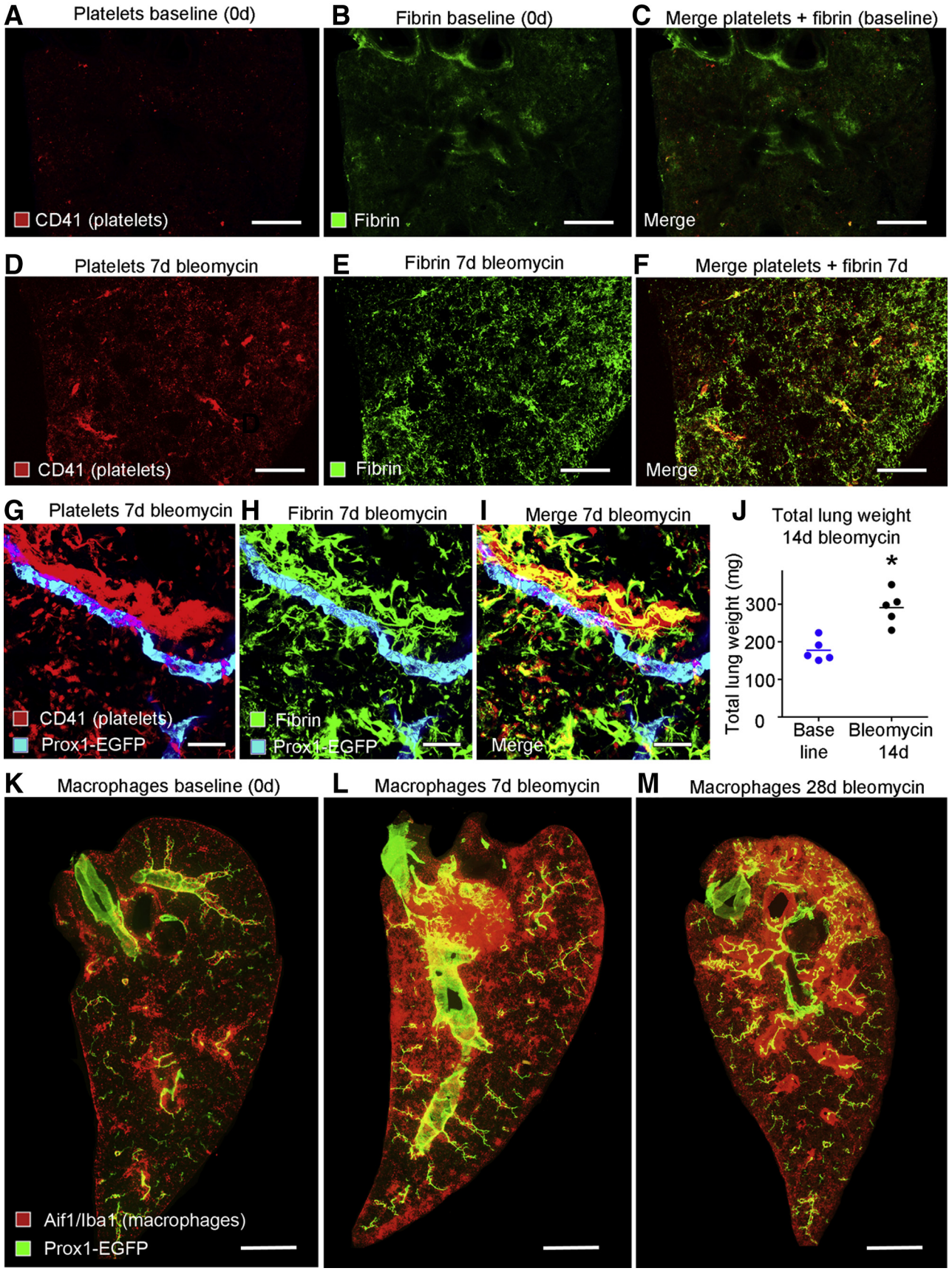
A
Platelets baseline (0d)
CD41 (platelets)
B
Fibrin baseline (0d)
Fibrin
C
Merge platelets + fibrin (baseline)
Merge
D
Platelets 7d bleomycin
CD41 (platelets)
E
Fibrin 7d bleomycin
Fibrin
F
Merge platelets + fibrin 7d
Merge
G
Platelets 7d bleomycin
CD41 (platelets)
Prox1-EGFP
H
Fibrin 7d bleomycin
Fibrin
Prox1-EGFP
I
Merge 7d bleomycin
Merge
J
Total lung weight
14d bleomycin
Total lung weight (mg)
300
200
100
0
*
Base line
Bleomycin 14d
K
Macrophages baseline (0d)
Aif1/Iba1 (macrophages)
Prox1-EGFP
L
Macrophages 7d bleomycin
M
Macrophages 28d bleomycin

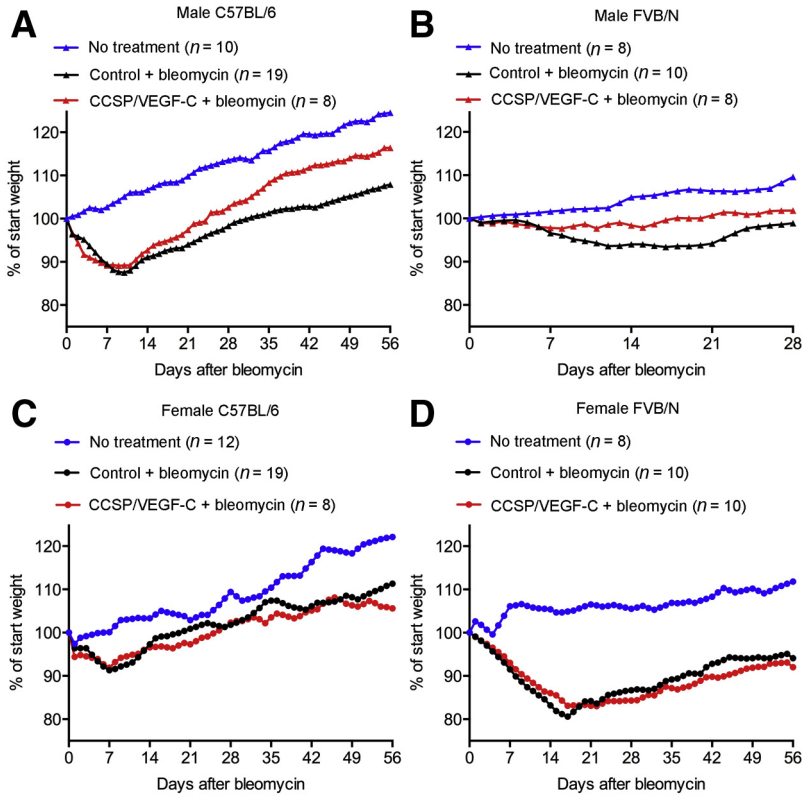

Figure 7 Influence of lymphatic network expansion, sex, and mouse strain on body weight recovery after bleomycin challenge. **A** and **B:** Comparison of body weight changes after challenge bleomycin in male controls and CCSP/VEGF-C transgenic mice in C57BL/6 and FVB/N backgrounds. Although male C57BL/6 mice had greater weight loss than male FVB/N mice, mice with lymphatic network expansion in both backgrounds had significantly faster recovery after bleomycin administration than corresponding controls ($P < 0.0004$, Kolmogorov-Smirnov test). Symbols represent means of groups. **C** and **D:** Body weight changes after bleomycin treatment in female mice in C57BL/6 and FVB/N backgrounds. Female FVB/N mice had greater weight loss than female C57BL/6 mice, but recovery after bleomycin treatment in females was slower than in males and was not significantly different in controls and CCSP/VEGF-C mice.

Preferential Lymphatic Growth in Regions of Extravasated Plasma

Lymphatic growth can be driven by multiple blood components. Human platelets release VEGF-C,[47,48] plasmin promotes maturation of VEGF-C into the fully active form by proteolytic cleavage,[45] and fibrin in extracellular matrix facilitates lymphatic growth.[49] The contributions of these factors to lymphangiogenesis after bleomycin challenge led to determining whether the expansion of the lung lymphatic network occurred preferentially in regions of plasma leakage. Fibrin and platelets, marked by immunohistochemical staining, were sparse or absent in normal lungs (Figure 6, A–C) but were abundant at 7 days after bleomycin administration (Figure 6, D–F), consistent with a contribution of Vegfc to subsequent lymphangiogenesis. Accumulations of fibrin and platelets coincided with regions of dense lymphatics (Figure 6, G–I). At 14 days, lung weight was increased by 64% ± 11% (Figure 6J), consistent with greater vascular leakage, edema, and cell influx.

Relationship of Lymphangiogenesis to Myeloid Cells

The distribution of myeloid cells was first evaluated as potential drivers of lymphatic growth and lung fibrosis by immunohistochemical staining of macrophages and dendritic cells using Aif1/Iba1 as a convenient marker,[50] and staining neutrophils for S100a8. In our hands, Aif1/Iba1 stained similar but not identical cell populations as antibodies to Cx3Cr1-EGFP and mannose receptor Mrc1. Aif1/Iba1 stained interstitial macrophages and dendritic cells, but not monocytes or alveolar macrophages, whereas Cx3cr1-EGFP and Mrc1 additionally marked monocytes and alveolar macrophages, respectively (Supplemental Figure S6A). This cellular localization for Aif1/Iba1 is consistent

Figure 6 Platelets, fibrin, and macrophages in lungs after bleomycin challenge. **A–F:** Low-magnification images of lungs comparing little or no staining for platelets (red; CD41) or fibrin (green; antifibrinogen/fibrin) at baseline (no bleomycin; **A–C**) with widespread staining for both at 7 days after bleomycin treatment (**D–F**), a stage in disease progression before much lymphangiogenesis has occurred. **G–I:** Higher-magnification images showing lymphatics (cyan) near overlapping deposits of platelets and fibrin. **J:** Wet lung weight (both lungs). Dots represent individual mice. Blue dots, baseline (no bleomycin); black dots, 14-day bleomycin. **K–M:** Macrophages (red) and prospero homeobox 1-enhanced green fluorescent protein (Prox1-EGFP) (green) in lymphatics and cardiac muscle of large pulmonary veins at 0, 7, and 28 days after bleomycin administration. **K:** Macrophages scarce at baseline. **L:** Increase in number 7 days after bleomycin treatment, preceding lymphatic growth. **M:** Macrophages coincident with regions of lymphatic growth at 28 days. $n = 5$ mice per group (**J**). *$P < 0.05$ versus baseline (t-test). Scale bars: 1 mm (**A–F** and **K–M**); 50 μm (**G–I**). Aif1/Iba1, allograft inflammatory factor 1/ionized calcium binding adapter molecule 1.

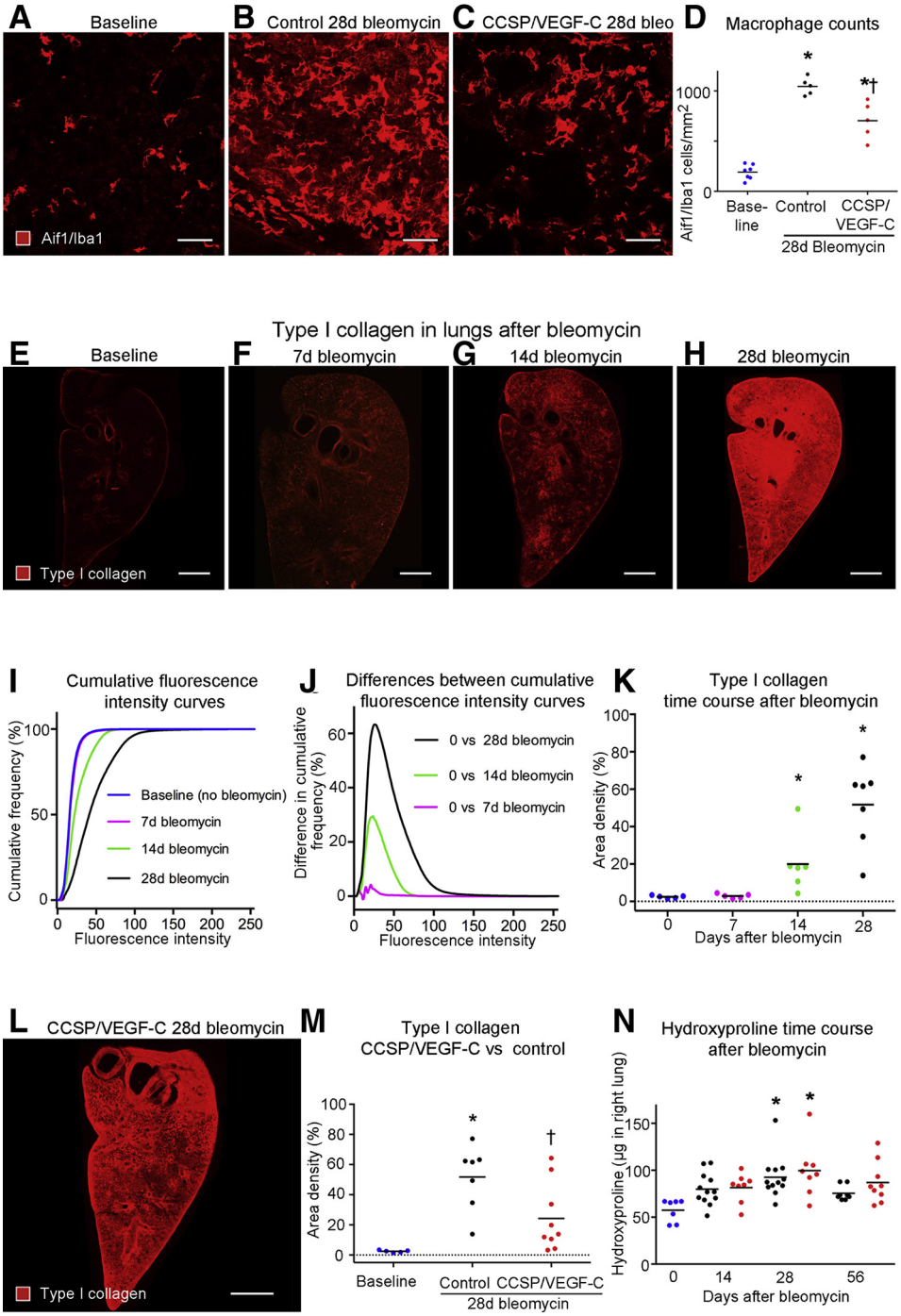

Figure 8 Fewer macrophages and less fibrosis after bleomycin challenge in lungs with expanded lymphatics. **A**—**C:** Staining of macrophages for allograft inflammatory factor 1/ionized calcium binding adapter molecule 1 (Aif1/Iba1). **D:** Counts of macrophages in hot spots in lung parenchyma after bleomycin administration. Macrophage numbers significantly increased in hot spots after bleomycin treatment, but significantly less in CCSP/VEGF-C lungs than in control lungs. **E**—**H:** Low-magnification panoramas of left lung of C57BL/6 mice stained for type I collagen, showing weak staining at baseline (**E**). After bleomycin challenge, staining is weak at 7 days (**F**), patchy at 14 days (**G**), and uniformly strong at 28 days (**H**). **I:** Measurements of type I collagen staining plotted as cumulative frequency of immunofluorescence pixel intensities in images at baseline and 7, 14, or 28 days after bleomycin challenge (**E**—**H**). Curves for 14 and 28 days significantly different from baseline. **J:** Relative amounts of type I collagen shown by height of curves plotted from group-related differences in cumulative frequencies from **I**. Taller curves indicate larger differences. **K:** Amounts of type I collagen in lungs of groups in **I** and **J** compared by area density measurements at threshold = 30 based on maximal difference in curves. **Dotted line**: zero on *y* axis. **L:** Less type I collagen staining at 28 days after bleomycin challenge in the lung of CCSP/VEGF-C mouse with expanded lymphatic network than in control mouse (**H**). **M:** Measurements of type I collagen staining in lungs as in **K**, comparing large increase at 28 days after bleomycin challenge in control mice with a significantly smaller increase in CCSP/VEGF-C mice. **Dotted line**: zero on *y* axis. **N:** Measurements of hydroxyproline in right lungs, showing increase over baseline group at 28 days after bleomycin challenge. Dots represent individual mice. Blue dots, baseline (no treatment). However, no significant difference was found between controls (black dots) and CCSP/VEGF-C mice (red dots). $n = 5$ to 7 mice per group (**D**); $n = 4$ to 7 mice per group (**J**); $n = 5$ to 12 mice per group (**N**). $^{*}P < 0.05$ versus baseline [analysis of variance (ANOVA)]; $^{\dagger}P < 0.05$ versus control (ANOVA). Scale bars: 50 μm (**A**—**C**); 1 mm (**E**—**H** and **L**).

with results from small conditional RNA-sequencing studies of mouse lungs reported (*www.immgen.org* and *https://tabula-muris.ds.czbiohub.org*, last accessed May 8, 2020). An unexpected finding regarding lung lymphatics was the presence of Mrc1 on initial lymphatics (Supplemental Figure S6B). This result was consistent with a suggested role for Mrc1 in immune cell entry into lymphatics.[51]

Macrophages were relatively scarce in baseline lungs, and were largely restricted to the walls of large airways and pulmonary blood vessels, with some in the lung visceral pleura (Figure 6K). By 7 days after bleomycin treatment, the number of macrophages increased, with focal densities near the lung hilum and pleura (Figure 6L). At this time, there was little lymphatic growth, as evidenced by Prox1-EGFP staining. At later time points (eg, 28 days), accumulations of macrophages coincided with regions of lymphatic growth (Figure 6M).

To document the time course of changes of myeloid cells in mouse lungs after bleomycin treatment, mRNA expression values of key marker genes were retrieved from published pan-genome studies of mouse lungs after bleomycin challenge.[40,41] These studies showed that macrophage markers peaked early after bleomycin injury and remained elevated throughout the disease (Supplemental Figure S7, A and B). In comparison, gene expression of markers of dendritic cells and neutrophils was more modestly increased. Expression of myeloid cell markers was also modestly increased in lungs of telomere-deficient mice (Supplemental Figure S7C).

Lung Lymphatic Network Expansion in CCSP/VEGF-C Mice

The effects of expansion of the lymphatic network on subsequent lung injury and fibrosis after bleomycin challenge were examined in adult double-transgenic CCSP/VEGF-C mice (C57BL/6 strain), where lymphangiogenesis in the lung is driven by Vegfc overexpression.[35,36] After CCSP/VEGF-C mice received doxycycline for 7 days, lung lymphatics were doubled in abundance (Supplemental Figure S8). Much of the lymphatic expansion was in the lung hilum around large airways, where Vegfc was secreted from CCSP-expressing epithelial cells; lymphatic expansion was less in the lung parenchyma (Supplemental Figure S8). Lung lymphatics underwent similar expansion in CCSP/VEGF-C mice bred in the FVB/N strain.

Readouts Unchanged by Lymphatic Network Expansion

Some measures of lung inflammation after bleomycin treatment in CCSP/VEGF-C mice (C57BL/6 strain) were similar to their single transgenic controls. In mice of both genotypes, BALF protein, an index of lung plasma leakage, peaked at 7 to 14 days; BALF leukocytes, an index of inflammatory cell influx, peaked at 14 days; and lymph node weight peaked at 14 to 28 days (Supplemental Figure S9, A–C). At 56 days, all values were less than the peak but still above baseline. No consistent differences were evident between CCSP/VEGF-C mice and their single transgenic controls. CCSP/VEGF-C mice bred in the FVB/N strain had more severe and prolonged responses to bleomycin challenge, but BALF values and lymph node weights were not significantly different from single transgenic controls (Supplemental Figure S9, D–F).

More Rapid Recovery with Lymphatic Network Expansion

Body weight decreased over the first 7 to 14 days after bleomycin challenge and then recovered to a variable extent. The rate of recovery varied with mouse sex, genotype, and strain. Male CCSP/VEGF-C mice of the C57BL/6 strain had about the same weight loss as their single transgenic controls but recovered more quickly (Figure 7A). Male CCSP/VEGF-C FVB/N mice not only lost less weight initially but also had a faster recovery than their single transgenic controls (Figure 7B). By comparison, C57BL/6 females of CCSP/VEGF-C and single transgenic genotypes lost less weight than FVB/N females and returned to their onset weight by 28 days (Figure 7C). FVB/N females of both genotypes lost more weight than any other mice; both genotypes gradually recovered but at 56 days were still below their onset weight (Figure 7D).

Fewer Macrophages and Reduced Fibrosis in Mice with Lymphatic Network Expansion

To assess the effect of lymphatic network expansion in lungs of CCSP/VEGF-C mice given bleomycin on myeloid cell influx, the numbers of Aif1/Iba1-positive macrophages and S100a8-positive neutrophils in hot spots in the lung parenchyma of fibrotic control and CCSP/VEGF-C lungs at 28 days after bleomycin challenge were compared. As expected, macrophage numbers were markedly increased relative to baseline lungs in both control and CCSP/VEGF-C lungs (Figure 8, A–D). However, the increase was significantly greater in control than in CCSP/VEGF-C lungs (5.4 versus 3.7 fold; $P < 0.05$, analysis of variance) (Figure 8D). Thus, macrophage density in hot spots in parenchyma of CCSP/VEGF-C lungs was reduced by 33% compared with control lungs. In contrast, the distribution of S100a8-positive neutrophils in bleomycin-treated lungs did not show marked focal accumulations, and neutrophil numbers were not significantly different in control versus CCSP/VEGF-C lungs (Supplemental Figure S10).

Impact of Lymphatic Expansion on Lung Fibrosis

CCSP/VEGF-C mice, previously given doxycycline at weaning to induce lymphatic expansion, were given bleomycin as adults, and fibrosis was assessed using type I collagen immunoreactivity. CCSP/VEGF-C mice had less fibrosis than their single transgenic controls at 28 days. Most type I collagen staining in normal baseline lungs was near large airways and blood vessels (Figure 8E). The amount of type I collagen staining increased after bleomycin treatment (Figure 8, F–H). At 7 days, most lung regions had little type I collagen staining (Figure 8F). By comparison, type I collagen staining was moderate in patchy regions at

14 days (Figure 8G) and at 28 days was strong throughout the lung (Figure 8H). Measurements expressed as the proportion of pixels over the range of fluorescence intensities reveal the time course of increases in type I collagen from onset to 28 days (Figure 8, I and J). Area density measurements confirmed significant increases in type I collagen at 14 and 28 days (Figure 8K). Although lungs of CCSP/VEGF-C mice at 28 days after bleomycin challenge had greater than normal staining for type I collagen (Figure 8L), importantly, the amount was significantly less than in single transgenic controls (Figure 8M).

Measurements of hydroxyproline proved less sensitive than type I collagen staining, which was not only specific for type I collagen but also revealed the regional distribution. Hydroxyproline values were greater at 14 days after bleomycin administration, peaked at 28 days, and at 56 days returned to the 14-day level. The values were highly variable and were not significantly different in lungs of CCSP/VEGF-C mice and their single transgenic controls (Figure 8N).

Discussion

To our knowledge, this is the first systematic study of the influence of lymphatics on the development of pulmonary fibrosis in two different mouse models. After intratracheal instillation of bleomycin, the lymphatic network expanded around large airways and blood vessels and in the lung parenchyma. Lymphatic growth was conspicuous at 14 days, peaked at 28 days, and was significantly less at 56 days, changes that paralleled the amount of fibrosis. Mechanistic studies revealed that Vegfc derived from macrophages was the driver of lymphatic growth after bleomycin challenge via Vegfr3 signaling. Lymphangiogenesis occurred preferentially at regions of inflammation characterized by plasma extravasation marked by accumulation of platelets and fibrin and infiltration by macrophages. Blocking of Vegfr3 signaling almost completely prevented lymphatic growth, but did not noticeably change the response to bleomycin during the first 14 days. However, CCSP/VEGF-C mice with an expanded lymphatic network had fewer macrophages in hot spots of inflamed lung parenchyma and had less fibrosis and faster recovery from disease.

Pattern of Lymphatic Growth after Lung Injury

The patterns of lymphatic growth after bleomycin-induced lung injury and in lungs with telomere dysfunction had certain similarities and differences. In both models, lymphangiogenesis occurred in regions of inflamed lung parenchyma that normally contain few lymphatics, as is the case in healthy human lungs.[20,21,52] In another similarity, lymphatic growth was also extensive around large airways and blood vessels after bleomycin treatment and in SPC-Cre/TRF1-floxed mice, but less so in CCSP-Cre/TRF1-floxed mice. Enlargement of collecting lymphatics in these regions is consistent with greater fluid drainage accompanying plasma leakage that is a well-documented consequence of bleomycin-induced lung injury.[53] Both models showed not only morphologic evidence of lymphatic growth but also increased *Prox1* and *Vegfr3* expression in the lungs. A major difference between the two models was in the time course and reversibility of lymphatic remodeling. In the bleomycin model, the peak of lymphatic growth at 14 to 28 days coincided with maximum lung inflammation,[29–32] followed by slow reversal. In contrast, in the telomere-deficient model, lymphatic growth occurred much more slowly and progressively.

Mouse versus Human Lung Lymphatics

Changes in lung lymphatics have been reported in many human lung parenchymal diseases, including idiopathic pulmonary fibrosis.[19–22,54] Despite the overall similarity in lymphatic architecture in mouse and human lungs,[52,55] direct comparisons are complicated by differences in expression of lymphatic marker molecules[56] and methods of visualizing and sampling lymphatics over the course of the disease. Mouse lungs usually have few lymphatics in their visceral pleura, at least at baseline, whereas pleural lymphatics are conspicuous in human lungs. Although the bleomycin model has been criticized as not fully mimicking human idiopathic pulmonary fibrosis,[33] some lessons learned from it may apply to human lungs.

Distribution of Lymphatic Growth after Lung Injury

The close spatial and temporal association of lymphatic growth after bleomycin challenge with hallmarks of inflammation gives us clues as to the possible causal mechanisms. In addition to macrophages, platelets are also a potential source of Vegfc.[47,48] Secreted Vegfc requires proteolytic maturation for its full activation,[44,45,57] and this can be provided by plasma proteases.[5,57] Fibrin can also facilitate lymphatic growth.[49] The growth of pleural lymphatics in mice could result from excess Vegfc that enters the pleural fluid and can lead to chylothorax in neonatal CCSP/VEGF-C mice.[36] Another conspicuous feature of lymphatic growth after bleomycin treatment was its association with diffuse clusters of lymphocytes and regions of bronchus-associated lymphoid tissue that represented anatomically well-developed tertiary lymphoid organs. These are known to develop after lung injury in mice and humans.[23–25,58,59] The finding of lymphocytes and myeloid cells within lung lymphatics suggests ongoing immune cell entry and transport toward the draining lymph nodes.

Mechanism of Lymphatic Growth after Lung Injury

Inhibition of Vegfr3 by function-blocking antibody during and after bleomycin challenge largely prevented the growth of lymphatics in the lung. This finding fits with other evidence for Vegfr3 signaling as the main driving force for lymphangiogenesis in models of inflammation,[5,7] including

Mycoplasma pulmonis infection.[23] Vegfc and Vegfd are the known ligands for Vegfr3.[5,45,60] Studies of gene and protein expression revealed that *Vegfc* but not *Vegfd* increased, providing further evidence for Vegfc/Vegfr3 signaling as the dominant driving mechanism for lymphangiogenesis after bleomycin challenge. Our data for Vegfc expression are consistent with values found in pan-genome microarray studies of mouse lungs after bleomycin challenge[40,41] or telomere dysfunction.[1]

Regions of lymphatic growth in the lung after bleomycin challenge were also marked by increased expression of *Ccl21*. In addition to Ccl21 staining in lymphatic endothelial cells themselves at baseline, after bleomycin challenge, Ccl21 was diffusely distributed around lymphatics in the parenchyma. Increased expression of *Ccl21* was also reported in mice with telomere dysfunction.[1] Ccl21 in lymphatic endothelial cells promotes immune cell trafficking into lymphatics by functioning as the ligand for Ccr7 on lymphocytes.[61,62] The finding of increased *Ccl21* expression after bleomycin administration is consistent with reports of Ccl21 induction by Vegfc/Vegfr3 signaling and secretion into the extracellular matrix, where it forms a chemotactic gradient for immune cell entry into lymphatics.[61–64]

Because immune cells are the likely source of Vegfc driving lymphatic growth, inhibition of Vegfr3 signaling by the blocking antibody may have reduced lymphatic growth in two ways: one, a direct action on Vegfr3 receptors on lymphatics, and another more indirect mechanism by reducing expression of *Ccl21*, thereby reducing chemotaxis for immune cells driving lymphatic growth. Consistent with this is the observation that deletion of *Ccr7* reduces inflammation and fibrosis in mouse lungs at 21 days after bleomycin challenge.[65]

Our results highlight the importance of macrophages as the drivers not only of fibrosis but also of lymphangiogenesis. Lymphatic growth followed the spatial and temporal influx of macrophages (but not neutrophils), and macrophages were identified were identified as a cellular source of VEGF. Our findings of increased macrophage density also agree with a report that mRNA for Aif1/Iba1 is increased approximately fourfold in mouse lungs at 28 days after bleomycin treatment.[50]

Reversibility of Lymphatic Growth

The reversibility of bleomycin-induced lung injury model made it possible to determine whether lymphatics regressed during resolution. Our finding of a slow but incomplete regression of newly formed lymphatics involving caspase-3–dependent apoptosis between days 28 and 56 after bleomycin treatment is consistent with a report that inflammatory cell influx peaked at 28 days and then gradually subsided, but never fully reversed.[32] This partial regression of lung lymphatics in the bleomycin model differs from their survival in mouse lungs after elimination of bacterial infection with antibiotics[23] or long-lasting lymphatics observed after transgenic activation of VEGF-C in neonatal mice.[36] In contrast, the pathologic changes in lungs with telomere dysfunction were progressive, irreversible, and fatal at about 1 year of age.[34]

Lymphatics and immune cells likely provide chemotactic, growth, and survival factors to each other in a reciprocal relationship.[6,43,64,66] However, the precise factors regulating lymphatic survival or regression are currently incompletely understood. For example, VEGF-C is required for the maintenance of lymphatics in intestinal villi of adult mice, but not for other lymphatics.[67] Likewise, when transgenic expression of VEGF-C in bone is switched off, ectopic lymphatics growing within the bone regress, but those growing in the surrounding muscle survive.[68] Lymphatic development in skin suggests the survival factors include the relative age and maturity of lymphatic endothelial cells concerned, fluid flow within the lymphatics, and sphingosine 1 phosphate receptor 1 and VEGFR-3 signaling.[69]

Mouse Strain and Sex-Related Differences

Mouse strain–related differences in disease severity after bleomycin challenge are well documented in the literature.[70,71] We originally developed CCSP/VEGF-C mice in the FVB/N strain,[36] but recognizing that data on FVB/N mice after bleomycin administration were more limited than for C57BL/6 mice,[72] CCSP/VEGF-C mice of both strains were compared. FVB/N mice proved more susceptible to bleomycin injury than C57BL/6 mice but had a different response. Both C57BL/6 and FVB/N strains had robust growth of lung lymphatics after bleomycin challenge, but FVB/N mice had greater lymph node enlargement and mortality, despite showing less weight loss. The absence of consistent differences in protein and leukocytes in BALF between CCSP/VEGF-C mice and control mice after bleomycin treatment indicates that these readouts are influenced more by changes in lung blood vessels than in lung lymphatics. Our experiments revealed that male CCSP/VEGF-C mice consistently recovered more quickly after bleomycin challenge than single transgenic controls. More rapid recovery of body weight was found in males of both C57BL/6 and FVB/N mouse strains, despite differences in disease severity and progression. Consistent with other reports,[70,71] male mice of both strains had a more severe response to bleomycin administration than females. Female CCSP/VEGF-C mice did not show the accelerated recovery found in males.

Prior Lymphatic Network Expansion Reduces Macrophage Numbers and Fibrosis and Accelerates Recovery from Lung Injury

Although lungs with expanded lymphatic networks had variable amounts of fibrosis, as reflected by hydroxyproline measurements, they contained significantly less type I collagen compared with control lungs. The apparent discrepancy between immunohistochemical measurements of type I collagen and hydroxyproline can be explained by differing specificities of the assays, where the antibody recognized only type I

collagen, but the biochemical assay measured hydroxyproline in all types of collagen. Type V collagen is known to increase in lungs after bleomycin challenge along with type I collagen,[40] and type IV collagen is abundant throughout the lung as the main constituent of basement membranes.

Recognition of lymphatic stasis may be a key point in understanding how lymphatic growth and function are linked to fibrosis. At baseline, efficient clearance of fluid and cells from the lung occurs through lymphatics. However, in severe inflammation, lymphatic clearance may be insufficient, leading to lymph stasis, which, in turn, is accompanied by fibrosis. Because fibrosis is a consequence of disordered wound healing, its severity increases with the intensity and duration of injury and decreases with faster resolution of the initial stimulus.[73–75] Fibrosis accompanies sustained lymph insufficiency in the heart,[12,13] liver,[76,77] skin,[7,78] and kidney,[79,80] and fibrosis is exaggerated by ligation of kidney lymphatics.[81] Other clinical examples of lymph stasis leading to fibrosis include limb lymphedema after removal of lymph nodes for breast cancer and elephantiasis after filarial infection.[9]

Experimental lymphatic network expansion can increase fluid drainage, as shown by more rapid clearance of fluorescent tracers, labeled antigens, or immune cells.[7] Lymphatic network expansion increases immune cell trafficking to lymph nodes, reduces inflammation and fibrosis, and improves recovery after myocardial infarction in mice.[12,13] Vegfc-driven lymphatic growth also reduces disease severity in models of rheumatoid arthritis, skin inflammation, and inflammatory bowel disease.[6,7]

The contribution to the amelioration of fibrosis of reversing lymph stasis by lymphatic network expansion and increased lymphatic clearance is not as well understood after lung injury as for other pathologic conditions. However, clues come from reports published during the early days of lung transplantation of reduced lung congestion in reimplanted lungs coinciding with lymphatic regeneration and anastomosis.[82,83] In our study, widespread extravasation of platelets and fibrinogen and the large increase in lung weight after bleomycin challenge reflect an excess accumulation of fluid and cells and insufficient lymphatic clearance. Together, our findings that lung lymphatic network expansion in CCSP/VEGF-C mice reduces lymph stasis, decreases fibrosis, and accelerates recovery from disease by increasing lymphatic clearance of fluid and cells are consistent with the mechanisms elucidated in other disease models.[6,66,84]

A key finding of our study was the correlation of lymphatic growth, macrophage density, and fibrosis. More important, macrophage accumulation was significantly less in lungs of CCSP/VEGF-C mice (with prior induced extra lymphatics) than in control lungs. The percentage reduction of macrophage numbers and fibrosis was similar in CCSP/VEGF-C mice after bleomycin challenge. These findings fit with a mechanism whereby the extra lymphatics accelerate the drainage of profibrotic macrophages from sites of inflammation. Increased expression of Ccl21, a chemotactic factor for myeloid cells from the additional lymphatics in CCSP/VEGF-C lungs, may mediate this effect.

In conclusion, widespread lymphatic growth occurs in pulmonary fibrosis after lung injury by bleomycin or in lungs with telomere dysfunction. Lymphatic growth after bleomycin challenge is driven by Vegfc from macrophages through Vegfr3 signaling and is accompanied by extravasation of platelets and fibrinogen and influx of other immune cells. We also conclude that prevention of lymphatic growth has little apparent effect on the development of lung injury after bleomycin treatment, but expansion of the lung lymphatic network in CCSP/VEGF-C mice before bleomycin injury reduces fibrosis and accelerates recovery by reducing lymph stasis and by increasing lymphatic clearance of fluid and cells, notably macrophage subsets that drive fibrosis.

Acknowledgments

We thank Mark Looney (University of California, San Francisco) for access to an automated veterinary hemocytometer; and Bronek Pytowski (Eli Lilly) for making available DC101 and mF4-31C1 blocking antibodies.

Author Contributions

P.B. designed and conducted studies, acquired and analyzed data, and wrote the manuscript; R.P.N. and P.J.W. provided telomere dysfunction mice, analyzed data, and wrote the manuscript; S.K. and F.R. acquired and analyzed data; D.C. conducted studies and acquired and analyzed data; Y.K.H. designed studies and analyzed data; D.M.M. designed studies and wrote the manuscript.

Supplemental Data

Supplemental material for this article can be found at *http://doi.org/10.1016/j.ajpath.2020.08.018*.

References

1. Aran D, Looney AP, Liu L, Wu E, Fong V, Hsu A, Chak S, Naikawadi RP, Wolters PJ, Abate AR, Butte AJ, Bhattacharya M: Reference-based analysis of lung single-cell sequencing reveals a transitional profibrotic macrophage. Nat Immunol 2019, 20:163–172
2. McCubbrey AL, Barthel L, Mohning MP, Redente EF, Mould KJ, Thomas SM, Leach SM, Danhorn T, Gibbings SL, Jakubzick CV, Henson PM, Janssen WJ: Deletion of c-FLIP from CD11b(hi) macrophages prevents development of bleomycin-induced lung fibrosis. Am J Resp Cell Mol Biol 2018, 58:66–78
3. Misharin AV, Morales-Nebreda L, Reyfman PA, Cuda CM, Walter JM, McQuattie-Pimentel AC, et al: Monocyte-derived alveolar macrophages drive lung fibrosis and persist in the lung over the life span. J Exp Med 2017, 214:2387–2404
4. Tsukui T, Sun KH, Wetter JB, Wilson-Kanamori JR, Hazelwood LA, Henderson NC, Adams TS, Schupp JC, Poli SD, Rosas IO, Kaminski N, Matthay MA, Wolters PJ, Sheppard D: Collagen-producing lung cell atlas identifies multiple subsets with distinct localization and relevance to fibrosis. Nat Commun 2020, 11:1920

5. Aspelund A, Robciuc MR, Karaman S, Makinen T, Alitalo K: Lymphatic system in cardiovascular medicine. Circ Res 2016, 118:515−530
6. Oliver G, Kipnis J, Randolph GJ, Harvey NL: The lymphatic vasculature in the 21(st) century: novel functional roles in homeostasis and disease. Cell 2020, 182:270−296
7. Schwager S, Detmar M: Inflammation and lymphatic function. Front Immunol 2019, 10:308
8. Jiang X, Nicolls MR, Tian W, Rockson SG: Lymphatic dysfunction, leukotrienes, and lymphedema. Annu Rev Physiol 2018, 80:49−70
9. Mortimer PS, Rockson SG: New developments in clinical aspects of lymphatic disease. J Clin Invest 2014, 124:915−921
10. Rockson SG, Tian W, Jiang X, Kuznetsova T, Haddad F, Zampell J, Mehrara B, Sampson JP, Roche L, Kim J, Nicolls MR: Pilot studies demonstrate the potential benefits of antiinflammatory therapy in human lymphedema. JCI Insight 2018, 3:e123775
11. Alexander JS, Chaitanya GV, Grisham MB, Boktor M: Emerging roles of lymphatics in inflammatory bowel disease. Ann N Y Acad Sci 2010, 1207(Suppl):E75−E85
12. Henri O, Pouehe C, Houssari M, Galas L, Nicol L, Edwards-Levy F, Henry JP, Dumesnil A, Boukhalfa I, Banquet S, Schapman D, Thuillez C, Richard V, Mulder P, Brakenhielm E: Selective stimulation of cardiac lymphangiogenesis reduces myocardial edema and fibrosis leading to improved cardiac function following myocardial infarction. Circulation 2016, 133:1484−1497
13. Vieira JM, Norman S, Villa Del Campo C, Cahill TJ, Barnette DN, Gunadasa-Rohling M, Johnson LA, Greaves DR, Carr CA, Jackson DG, Riley PR: The cardiac lymphatic system stimulates resolution of inflammation following myocardial infarction. J Clin Invest 2018, 128:3402−3412
14. Louveau A, Herz J, Alme MN, Salvador AF, Dong MQ, Viar KE, Herod SG, Knopp J, Setliff JC, Lupi AL, Da Mesquita S, Frost EL, Gaultier A, Harris TH, Cao R, Hu S, Lukens JR, Smirnov I, Overall CC, Oliver G, Kipnis J: CNS lymphatic drainage and neuroinflammation are regulated by meningeal lymphatic vasculature. Nat Neurosci 2018, 21:1380−1391
15. Cui Y, Liu K, Monzon-Medina ME, Padera RF, Wang H, George G, Toprak D, Abdelnour E, D'Agostino E, Goldberg HJ, Perrella MA, Forteza RM, Rosas IO, Visner G, El-Chemaly S: Therapeutic lymphangiogenesis ameliorates established acute lung allograft rejection. J Clin Invest 2015, 125:4255−4268
16. D'Alessio S, Correale C, Tacconi C, Gandelli A, Pietrogrande G, Vetrano S, Genua M, Arena V, Spinelli A, Peyrin-Biroulet L, Fiocchi C, Danese S: VEGF-C-dependent stimulation of lymphatic function ameliorates experimental inflammatory bowel disease. J Clin Invest 2014, 124:3863−3878
17. Krebs R, Tikkanen JM, Ropponen JO, Jeltsch M, Jokinen JJ, Ylä-Herttuala S, Nykänen AI, Lemström KB: Critical role of VEGF-C/VEGFR-3 signaling in innate and adaptive immune responses in experimental obliterative bronchiolitis. Am J Pathol 2012, 181: 1607−1620
18. Kretschmer S, Dethlefsen I, Hagner-Benes S, Marsh LM, Garn H, Konig P: Visualization of intrapulmonary lymph vessels in healthy and inflamed murine lung using CD90/Thy-1 as a marker. PLoS One 2013, 8:e55201
19. Stump B, Cui Y, Kidambi P, Lamattina AM, El-Chemaly S: Lymphatic changes in respiratory diseases: more than just remodeling of the lung? Am J Resp Cell Mol Biol 2017, 57:272−279
20. Ebina M: Pathognomonic remodeling of blood and lymphatic capillaries in idiopathic pulmonary fibrosis. Resp Invest 2017, 55: 2−9
21. Ebina M, Shibata N, Ohta H, Hisata S, Tamada T, Ono M, Okaya K, Kondo T, Nukiwa T: The disappearance of subpleural and interlobular lymphatics in idiopathic pulmonary fibrosis. Lymphatic Res Biol 2010, 8:199−207
22. El-Chemaly S, Malide D, Zudaire E, Ikeda Y, Weinberg BA, Pacheco-Rodriguez G, Rosas IO, Aparicio M, Ren P, MacDonald SD, Wu HP, Nathan SD, Cuttitta F, McCoy JP, Gochuico BR, Moss J: Abnormal lymphangiogenesis in idiopathic pulmonary fibrosis with insights into cellular and molecular mechanisms. Proc Natl Acad Sci USA 2009, 106:3958−3963
23. Baluk P, Adams A, Phillips K, Feng J, Hong YK, Brown MB, McDonald DM: Preferential lymphatic growth in bronchus-associated lymphoid tissue in sustained lung inflammation. Am J Pathol 2014, 184:1577−1592
24. Silva-Sanchez A, Randall TD: Role of iBALT in respiratory immunity. Curr Top Microbiol Immunol 2020, 426:21−43
25. Reed HO, Wang L, Sonett J, Chen M, Yang J, Li L, Aradi P, Jakus Z, D'Armiento J, Hancock WW, Kahn ML: Lymphatic impairment leads to pulmonary tertiary lymphoid organ formation and alveolar damage. J Clin Invest 2019, 130:2514−2526
26. Outtz Reed H, Wang L, Kahn ML, Hancock WW: Donor-host lymphatic anastomosis after murine lung transplantation. Transplantation 2020, 104:511−515
27. Maisel K, Sasso MS, Potin L, Swartz MA: Exploiting lymphatic vessels for immunomodulation: rationale, opportunities, and challenges. Adv Drug Deliv Rev 2017, 114:43−59
28. Cabrera S, Selman M, Lonzano-Bolanos A, Konishi K, Richards TJ, Kaminski N, Pardo A: Gene expression profiles reveal molecular mechanisms involved in the progression and resolution of bleomycin-induced lung fibrosis. Am J Physiol Lung Cell Mol Physiol 2013, 304:L593−L601
29. Izbicki G, Segel MJ, Christensen TG, Conner MW, Breuer R: Time course of bleomycin-induced lung fibrosis. Int J Expl Pathol 2002, 83:111−119
30. Liu T, De Los Santos FG, Phan SH: The bleomycin model of pulmonary fibrosis. Methods Mol Biol 2017, 1627:27−42
31. O'Dwyer DN, Moore BB: Animal models of pulmonary fibrosis. Methods Mol Biol 2018, 1809:363−378
32. Limjunyawong N, Mitzner W, Horton MR: A mouse model of chronic idiopathic pulmonary fibrosis. Physiol Rep 2014, 2:e00249
33. Jenkins RG, Moore BB, Chambers RC, Eickelberg O, Konigshoff M, Kolb M, Laurent GJ, Nanthakumar CB, Olman MA, Pardo A, Selman M, Sheppard D, Sime PJ, Tager AM, Tatler AL, Thannickal VJ, White ES; ATS Assemby on Respiratory Cell and Molecular Biology: An official American Thoracic Society workshop report: use of animal models for the preclinical assessment of potential therapies for pulmonary fibrosis. Am J Res Cell Mol Biol 2017, 56:667−679
34. Naikawadi RP, Disayabutr S, Mallavia B, Donne ML, Green G, La JL, Rock JR, Looney MR, Wolters PJ: Telomere dysfunction in alveolar epithelial cells causes lung remodeling and fibrosis. JCI Insight 2016, 1:e86704
35. Baluk P, Yao LC, Flores JC, Choi D, Hong YK, McDonald DM: Rapamycin reversal of VEGF-C-driven lymphatic anomalies in the respiratory tract. JCI Insight 2017, 2:e90103
36. Yao LC, Testini C, Tvorogov D, Anisimov A, Vargas SO, Baluk P, Pytowski B, Claesson-Welsh L, Alitalo K, McDonald DM: Pulmonary lymphangiectasia resulting from vascular endothelial growth factor-C overexpression during a critical period. Circ Res 2014, 114: 806−822
37. Choi I, Chung HK, Ramu S, Lee HN, Kim KE, Lee S, Yoo J, Choi D, Lee YS, Aguilar B, Hong YK: Visualization of lymphatic vessels by Prox1-promoter directed GFP reporter in a bacterial artificial chromosome-based transgenic mouse. Blood 2011, 117: 362−365
38. Baluk P, McDonald DM: Imaging lymphatics in mouse lungs. Methods Mol Biol 2018, 1846:161−180
39. Della Latta V, Cabiati M, Burchielli S, Frenzilli G, Bernardeschi M, Cecchettini A, Viglione F, Morales MA, Del Ry S: Lung inflammation after bleomycin treatment in mice: selection of an accurate normalization strategy for gene expression analysis in an ex-vivo and in-vitro model. Int J Biochem Cell Biol 2017, 88:145−154
40. Blaauboer ME, Emson CL, Verschuren L, van Erk M, Turner SM, Everts V, Hanemaaijer R, Stoop R: Novel combination of collagen

dynamics analysis and transcriptional profiling reveals fibrosis-relevant genes and pathways. Matrix Biol 2013, 32:424–431
41. Peng R, Sridhar S, Tyagi G, Phillips JE, Garrido R, Harris P, Burns L, Renteria L, Woods J, Chen L, Allard J, Ravindran P, Bitter H, Liang Z, Hogaboam CM, Kitson C, Budd DC, Fine JS, Bauer CM, Stevenson CS: Bleomycin induces molecular changes directly relevant to idiopathic pulmonary fibrosis: a model for "active" disease. PLoS One 2013, 8:e59348
42. Tal O, Lim HY, Gurevich I, Milo I, Shipony Z, Ng LG, Angeli V, Shakhar G: DC mobilization from the skin requires docking to immobilized CCL21 on lymphatic endothelium and intralymphatic crawling. J Exp Med 2011, 208:2141–2153
43. Russo E, Teijeira A, Vaahtomeri K, Willrodt AH, Bloch JS, Nitschke M, Santambrogio L, Kerjaschki D, Sixt M, Halin C: Intralymphatic CCL21 promotes tissue egress of dendritic cells through afferent lymphatic vessels. Cell Rep 2016, 14:1723–1734
44. Bui HM, Enis D, Robciuc MR, Nurmi HJ, Cohen J, Chen M, Yang Y, Dhillon V, Johnson K, Zhang H, Kirkpatrick R, Traxler E, Anisimov A, Alitalo K, Kahn ML: Proteolytic activation defines distinct lymphangiogenic mechanisms for VEGFC and VEGFD. J Clin Invest 2016, 126:2167–2180
45. Jha SK, Rauniyar K, Jeltsch M: Key molecules in lymphatic development, function, and identification. Ann Anat 2018, 219:25–34
46. Sun KH, Chang Y, Reed NI, Sheppard D: alpha-Smooth muscle actin is an inconsistent marker of fibroblasts responsible for force-dependent TGFbeta activation or collagen production across multiple models of organ fibrosis. Am J Physiol Lung Cell Mol Physiol 2016, 310:L824–L836
47. Lim L, Bui H, Farrelly O, Yang J, Li L, Enis D, Ma W, Chen M, Oliver G, Welsh JD, Kahn ML: Hemostasis stimulates lymphangiogenesis through release and activation of VEGFC. Blood 2019, 134: 1764–1775
48. Wartiovaara U, Salven P, Mikkola H, Lassila R, Kaukonen J, Joukov V, Orpana A, Ristimaki A, Heikinheimo M, Joensuu H, Alitalo K, Palotie A: Peripheral blood platelets express VEGF-C and VEGF which are released during platelet activation. Thromb Haemost 1998, 80:171–175
49. Guc E, Briquez PS, Foretay D, Fankhauser MA, Hubbell JA, Kilarski WW, Swartz MA: Local induction of lymphangiogenesis with engineered fibrin-binding VEGF-C promotes wound healing by increasing immune cell trafficking and matrix remodeling. Biomaterials 2017, 131:160–175
50. Nagahara H, Seno T, Yamamoto A, Obayashi H, Inoue T, Kida T, Nakabayashi A, Kukida Y, Fujioka K, Fujii W, Murakami K, Kohno M, Kawahito Y: Role of allograft inflammatory factor-1 in bleomycin-induced lung fibrosis. Biochem Biophys Res Commun 2018, 495:1901–1907
51. Marttila-Ichihara F, Turja R, Miiluniemi M, Karikoski M, Maksimow M, Niemelä J, Martinez-Pomares L, Salmi M, Jalkanen S: Macrophage mannose receptor on lymphatics controls cell trafficking. Blood 2008, 112:64–72
52. Kambouchner M, Bernaudin JF: Intralobular pulmonary lymphatic distribution in normal human lung using D2-40 antipodoplanin immunostaining. J Histochem Cytochem 2009, 57:643–648
53. Parker JC: Acute lung injury and pulmonary vascular permeability: use of transgenic models. Compr Physiol 2011, 1:835–882
54. Ebina M: Remodeling of airway walls in fatal asthmatics decreases lymphatic distribution: beyond thickening of airway smooth muscle layers. Allergol Int 2008, 57:165–174
55. Weber E, Sozio F, Borghini A, Sestini P, Renzoni E: Pulmonary lymphatic vessel morphology: a review. Ann Anat 2018, 218: 110–117
56. Baluk P, McDonald DM: Markers for microscopic imaging of lymphangiogenesis and angiogenesis. Ann N Y Acad Sci 2008, 1131:1–12
57. Ristimaki A, Narko K, Enholm B, Joukov V, Alitalo K: Proinflammatory cytokines regulate expression of the lymphatic endothelial mitogen vascular endothelial growth factor-C. J Biol Chem 1998, 273:8413–8418
58. Yadava K, Bollyky P, Lawson MA: The formation and function of tertiary lymphoid follicles in chronic pulmonary inflammation. Immunology 2016, 149:262–269
59. Mori M, Andersson CK, Svedberg KA, Glader P, Bergqvist A, Shikhagaie M, Löfdahl CG, Erjefält JS: Appearance of remodelled and dendritic cell-rich alveolar-lymphoid interfaces provides a structural basis for increased alveolar antigen uptake in chronic obstructive pulmonary disease. Thorax 2013, 68:521–531
60. Stacker SA, Achen MG: Emerging roles for VEGF-D in human disease. Biomolecules 2018, 8:1
61. Vaahtomeri K, Brown M, Hauschild R, De Vries I, Leithner AF, Mehling M, Kaufmann WA, Sixt M: Locally triggered release of the chemokine CCL21 promotes dendritic cell transmigration across lymphatic endothelia. Cell Rep 2017, 19:902–909
62. Nykänen AI, Sandelin H, Krebs R, Keränen MA, Tuuminen R, Kärpänen T, Wu Y, Pytowski B, Koskinen PK, Ylä-Herttuala S, Alitalo K, Lemstrom KB: Targeting lymphatic vessel activation and CCL21 production by vascular endothelial growth factor receptor-3 inhibition has novel immunomodulatory and antiarteriosclerotic effects in cardiac allografts. Circulation 2010, 121:1413–1422
63. Issa A, Le TX, Shoushtari AN, Shields JD, Swartz MA: Vascular endothelial growth factor-C and C-C chemokine receptor 7 in tumor cell-lymphatic cross-talk promote invasive phenotype. Cancer Res 2009, 69:349–357
64. Iwami D, Brinkman CC, Bromberg JS: Vascular endothelial growth factor c/vascular endothelial growth factor receptor 3 signaling regulates chemokine gradients and lymphocyte migration from tissues to lymphatics. Transplantation 2015, 99:668–677
65. Trujillo G, Hartigan AJ, Hogaboam CM: T regulatory cells and attenuated bleomycin-induced fibrosis in lungs of CCR7-/- mice. Fibrogenesis Tissue Repair 2010, 3:18
66. Randolph GJ, Ivanov S, Zinselmeyer BH, Scallan JP: The lymphatic system: integral roles in immunity. Annu Rev Immunol 2017, 35:31–52
67. Nurmi H, Saharinen P, Zarkada G, Zheng W, Robciuc MR, Alitalo K: VEGF-C is required for intestinal lymphatic vessel maintenance and lipid absorption. EMBO Mol Med 2015, 7:1418–1425
68. Hominick D, Silva A, Khurana N, Liu Y, Dechow PC, Feng JQ, Pytowski B, Rutkowski JM, Alitalo K, Dellinger MT: VEGF-C promotes the development of lymphatics in bone and bone loss. Elife 2018, 7:e34323
69. Geng X, Yanagida K, Akwii RG, Choi D, Chen L, Ho Y, Cha B, Mahamud MR, Berman de Ruiz K, Ichise H, Chen H, Wythe J, Mikelis CM, Hla T, Srinivasan RS: S1PR1 regulates the quiescence of lymphatic vessels by inhibiting laminar shear stress-dependent VEGF-C signaling. JCI Insight 2020, 5:137652
70. Redente EF, Jacobsen KM, Solomon JJ, Lara AR, Faubel S, Keith RC, Henson PM, Downey GP, Riches DW: Age and sex dimorphisms contribute to the severity of bleomycin-induced lung injury and fibrosis. Am J Physiol Lung Cell Mol Physiol 2011, 301: L510–L518
71. Walkin L, Herrick SE, Summers A, Brenchley PE, Hoff CM, Korstanje R, Margetts PJ: The role of mouse strain differences in the susceptibility to fibrosis: a systematic review. Fibrogenesis Tissue Repair 2013, 6:18
72. Arras M, Louahed J, Heilier JF, Delos M, Brombacher F, Renauld JC, Lison D, Huaux F: IL-9 protects against bleomycin-induced lung injury: involvement of prostaglandins. Am J Pathol 2005, 166: 107–115
73. Distler JHW, Gyorfi AH, Ramanujam M, Whitfield ML, Konigshoff M, Lafyatis R: Shared and distinct mechanisms of fibrosis. Nat Rev Rheumatol 2019, 15:705–730
74. Glasser SW, Hagood JS, Wong S, Taype CA, Madala SK, Hardie WD: Mechanisms of lung fibrosis resolution. Am J Pathol 2016, 186:1066–1077

75. Horowitz JC, Thannickal VJ: Mechanisms for the resolution of organ fibrosis. Physiology 2019, 34:43−55
76. Tanaka M, Iwakiri Y: Lymphatics in the liver. Curr Op Immunol 2018, 53:137−142
77. Tamburini BAJ, Finlon JM, Gillen AE, Kriss MS, Riemondy KA, Fu R, Schuyler RP, Hesselberth JR, Rosen HR, Burchill MA: Chronic liver disease in humans causes expansion and differentiation of liver lymphatic endothelial cells. Front Immunol 2019, 10:1036
78. Ghanta S, Cuzzone DA, Torrisi JS, Albano NJ, Joseph WJ, Savetsky IL, Gardenier JC, Chang D, Zampell JC, Mehrara BJ: Regulation of inflammation and fibrosis by macrophages in lymphedema. Am J Physiol Heart Circ Physiol 2015, 308:H1065−H1077
79. Hasegawa S, Nakano T, Torisu K, Tsuchimoto A, Eriguchi M, Haruyama N, Masutani K, Tsuruya K, Kitazono T: Vascular endothelial growth factor-C ameliorates renal interstitial fibrosis through lymphangiogenesis in mouse unilateral ureteral obstruction. Lab Invest 2017, 97:1439−1452
80. Pedersen MS, Muller M, Rulicke T, Leitner N, Kain R, Regele H, Wang S, Grone HJ, Rong S, Haller H, Gueler F, Rees AJ, Kerjaschki D: Lymphangiogenesis in a mouse model of renal transplant rejection extends life span of the recipients. Kidney Int 2020, 97:89−94
81. Zhang T, Guan G, Liu G, Sun J, Chen B, Li X, Hou X, Wang H: Disturbance of lymph circulation develops renal fibrosis in rats with or without contralateral nephrectomy. Nephrology 2008, 13:128−138
82. Ruggiero R, Muz J, Fietsam R Jr, Thomas GA, Welsh RJ, Miller JE, Stephenson LW, Baciewicz FA Jr: Reestablishment of lymphatic drainage after canine lung transplantation. J Thorac Cardiovasc Surg 1993, 106:167−171
83. Thomas PA Jr: Physiologic sufficiency of regenerated lung lymphatics. Ann Surg 1980, 192:162−168
84. Kataru RP, Baik JE, Park HJ, Wiser I, Rehal S, Shin JY, Mehrara BJ: Regulation of immune function by the lymphatic system in lymphedema. Front Immunol 2019, 10:470